Topology and Control Method Development for Impedance Source Converter

A Dissertation submitted in fulfillment of the requirements for the Degree of

MASTER OF ENGINEERING

in

Power Systems

Submitted by

Subha Maiti
802042024

Under the Guidance of

Dr. Santosh Sonar
Assitant Professor, EIED

2022

Electrical and Instrumentation Engineering Department
Thapar Institute of Engineering & Technology, Patiala
(Declared as Deemed-to-be-University u/s 3 of the UGC Act., 1956)
Post Bag No. 32, Patiala – 147004
Punjab (India)

DECLARATION

I hereby certify that the work which is presented in the dissertation entitled, "Topology and Control Method Development for Impedance Source Converter", in fulfilment of the requirements for the award of the degree of Master of Engineering in Power Systems, submitted to the Electrical & Instrumentation Engineering Department of Thapar Institute of Engineering & Technology (Deemed to be University) is an as authentic record of my work carried under the supervision of Dr. Santosh Sonar. It refers to others researchers' work which is duly listed in the reference section. The matter contained in this dissertation has not been submitted, neither in part nor in full to any other degree to any other university or institute except as reported in text and references.

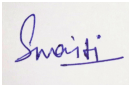

Place: Patiala **Subha Maiti**

Date: 5th September 2022 **Roll No.: 802042024**

It is certified that the above statement made by the student is correct to the best of my knowledge and belief.

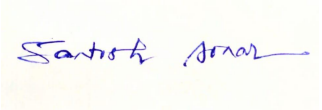

(Dr. Santosh Sonar)

Assistant Professor, EIED

ACKNOWLEDGEMENT

I would like to thank the Thapar Institute of Engineering and Technology, Patiala for giving me the opportunity to use their resources & work in an inspiring atmosphere.

First and foremost, I take this opportunity to express my deepest sense of gratitude to my guide **Dr. Santosh Sonar**, Assistant Professor, Thapar Institute of Engineering and Technology, Patiala, for his guidance during my dissertation work. This report would not have been possible without help and the valuable time that he has given me amidst his busy schedule. I thank **Mr. Lalit Singh,** Lab Technician, TIET Patiala for enormous supporting where ever needed. I also thank **Dr. Sanjoy Mondal** Assistant Professor, Institute of Engineering and Management (IEM), Kolkata, for his guidance and time.

I would like to express my deepest sense of gratitude towards **Dr. R. S. Kaler**, Senior Professor, and Head, EIED, Thapar Institute of Engineering and Technology, Patiala who has been a constant source of inspiration for me throughout the preparation.

I would also like to extend my gratitude to my parents and friends in this department who have always encouraged and supported me in doing my work.

Last but not least I would like to thank all the staff and faculty members of the department of Electrical and Instrumentation Engineering who have been very cooperative with me.

TABLE OF CONTENTS

LIST OF TABLES

LIST OF FIGURES

NOMENCLATURE

ABSTRACT

The improved characteristics of impedance source converters presented in recent literatures such as efficient power conversion, single stage buck-boost capability and reliability compared to voltage/current source inverters have made it a suitable candidate for a variety of distributed generation power applications. The limitations of VSI (voltage source inverter) and CSI (current source inverter) are removed by impedance source inverter (ZSI). It is well established that the null state included in the pulse width modulation scheme of a voltage source inverter is foundation for Z-Source inverter. There are mainly two states in the case of impedance source inverter, shoot-through and non-shoot-through states. In ST (shoot-through) the inductor charges and at NST (non-shoot-through) it discharges. In NST state, the inductor voltage adds up with the source voltage and a boosted output voltage is achieved. In this thesis, analysis of different control techniques, SBC (simple boost control), MBC (maximum boost control), and MCBC (maximum constant boost control) in terms of output voltages, total harmonic distortion, voltage stress, boost factor, and gain is discussed in detail. The core work of this thesis is the generation of ST pulses with three different control methods and their comparison, so that suitable control method can be selected for different applications. Simulation is carried out in MATLAB Simulink and results are presented to verify the mathematical findings. Different graphs have been plotted to highlight the merits/demerits of the proposed control techniques. Experimental results are presented to justify the theoretical and simulation results.

CHAPTER 1
INTRODUCTION

1. 1 INTRODUCTION TO CONVERTER

The circuit that converts DC to AC is referred to as an inverter. The motive is to produce an Alternating current (AC) voltage when only Direct current (DC) voltage is available. By changing the input DC voltage while keeping the inverter's gain constant, a variable output voltage may be achieved. Now if the DC voltage is fixed and not changeable, a variable output voltage can be generated by altering the gain of the inverter, which is often performed using Pulse width modulation (PWM) control within the inverter. The ratio of AC output voltage to DC input voltage is known as the inverter gain.

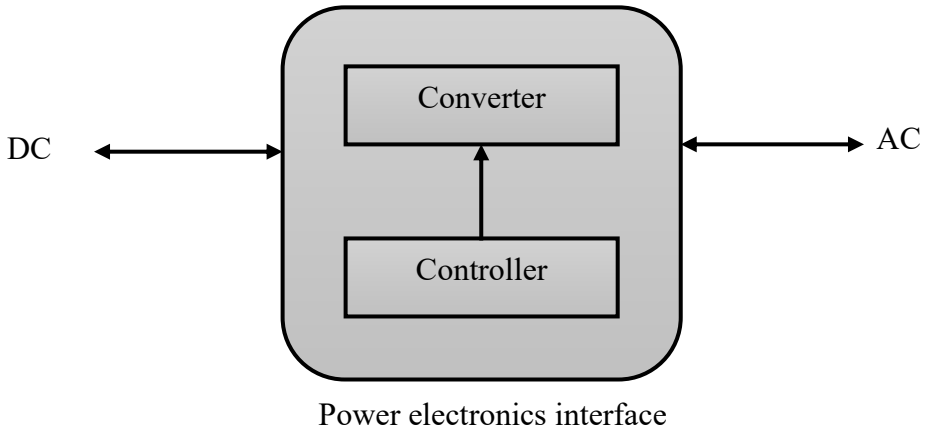

Figure 1. 1 Basic configuration of a power converter

Talking about in terms of power rating Figure 1.1 is very much different from the linear circuits. The power is measured in watts in the case of linear electronics, however talking about power electronics, it although measured in up to megawatts. Now, these power electronic devices carry up to several Kilo ampere (kA) in the case of forward bias conditions and case of reverse bias conditions blocks up to several Kilo Volt (kV). So, it must be designed like that so that it can withstand it. Metal Oxide Semiconductor Field Effect Transistor (MOSFET), Bipolar Junction Transistor (BJT), Insulated Gate Bipolar Transistor (IGBT), and Gate Turn-Off Thyristor (GTO) are only a handful of the numerous power semiconductors used in power electronics.

There are two types of classic inverters one is a Voltage source inverter (VSI) and another is a current source inverter (CSI).

1. 2 INVERTERS

In Power electronics, there are two classic inverters. One is VSI and another is CSI. Talking first of VSI there are several flaws followed by CSI. One of the notable flaws of VSI is that the output AC voltage obtained over here is less than that of input DC voltage. Similarly, in the case of CSI, the vice versa is there.

The second notable point is that VSI is given with a dead time, dead time is nothing but an additional time that is given to the switches so that they could be turned OFF properly and be safe from damage. Similarly talking about the CSI an over-lap time is given because we cannot keep open the switch in case of CSI, so for all time at least one switch from the top bank and another from the bottom bank must be ON.

The VSIs are mainly used in those places where the voltage is the main concern. Some of the applications are as follows: (I) UPS i.e., uninterruptable power supply. (II) Inverters are used in home applications (III) Photo Voltaic (PV) cell applications etc.

The CSIs are only used in those places where the current is the foremost concern. Some of the applications of the CSIs are: (I) Electric traction. (II) Induction motors (IM) for pumps. (III) AC motor drives etc.

Correspondingly, both the VSI and the CSI suffer the alike matters: (I) Buck, as well as Boost, cannot be feasible with a single inverter. It should be one at a time i.e., step up or step down. (II) We cannot exchange the internal circuits of these two converters. To put it simply, neither the VSI's main circuit can be used for the CSI, nor vice versa. A tree diagram of the Inverter is presented in Fig.1.2.

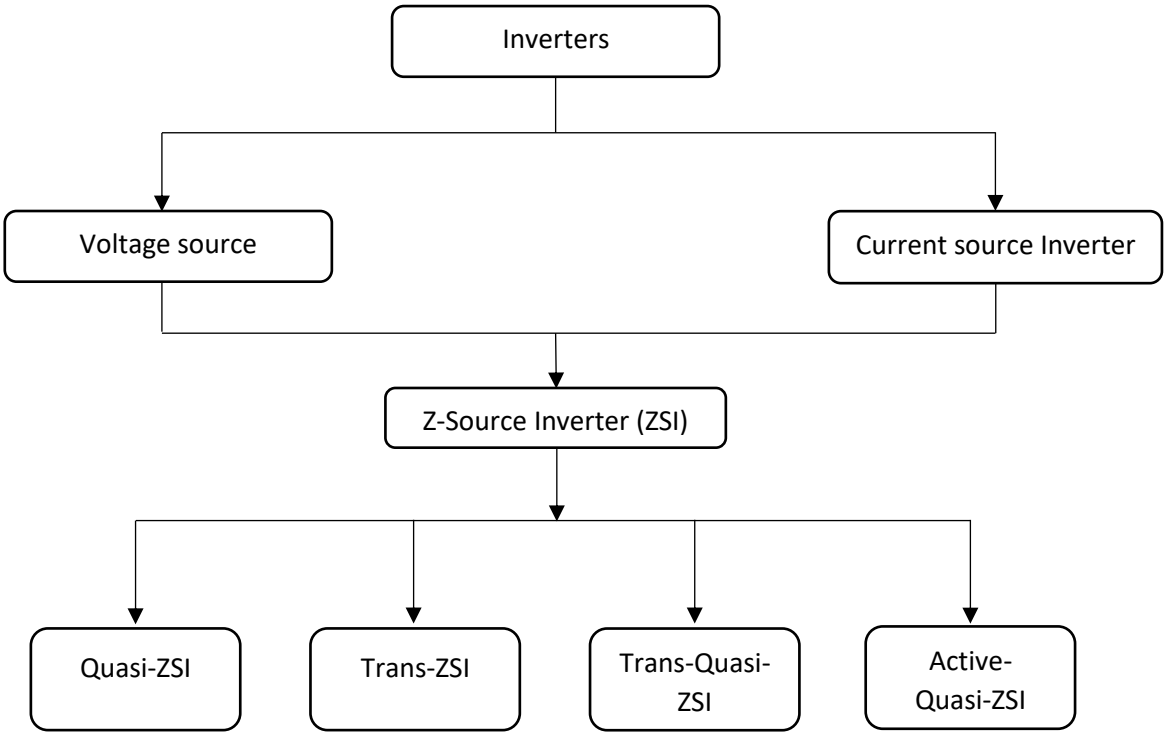

Figure 1. 2 Tree diagram of Inverter

A Z - source (ZSC) converter has been evolved to resolve these issues. Figure 1.2 describe the chart of the inverter's family. There are two classical inverters voltage source (VSI) and current source (CSI) inverters [7,8]. The advantages of both the inverters can be combined and Z-Source inverter (ZSI) is developed [1-3]. The Z-Source inverter again can be divided into mainly four categories as per the requirements and some added advantages. Those are Quasi-ZSI, Trans-ZSI, Trans-Quasi-ZSI, and Active-Quasi-ZSI. Each type of Z-Source inverter circuit is different from one other.

The thesis is organized as follows: Chapter – 2 presents the literature survey, Chapter – 3 deals with the research gap based on literature survey and objectives are defined, Chapter – 4 discusses the different topologies of ZSI, PWM techniques of ZSIs has been discussed in Chapter – 5 , Chapter – 6 presents detailed analysis of topologies and PWM techniques, Chapter – 7 comprises a second order sliding mode control algorithm ,Chapter – 8 presents simulation and experimental results Chapter – 9 concludes this thesis.

CHAPTER 2
LITERATURE SURVEY

Whenever there is a DC power available from different resources like solar, fuel-cell, etc. inverter is the most suitable device to obtain AC power [1-3]. Generally, in power electronics, we talk about two classic inverters i.e., the VSI and the other one is CSI [4]. It may be a three-phase or single-phase [5], depending upon the requirements. In power electronics whenever we talk about these two classic inverters we mostly talk about the single-phase or three-phase full-wave inverter. Nowadays IGBTs with diode anti-parallel or series depends upon the configuration i.e., whether it is a VSI or CSI is used [4-6]. In VSI we use a diode with anti-parallel with the switches i.e., here IGBTs. This is because if we talk about the resistive load then we know that the resistive load cannot store the energy but talk about the inductive load, then it will store energy i.e., the energy will tap inside it [7]. That's why an anti-parallel diode has been given over here so that the inductor can release energy from the diodes [7,8]. And here the voltage waveforms do not depend upon the load. Talking a bit about the CSI, here the switching sequence is very much different than the VSI for certain reasons [8]. Because here we intentionally short circuit the two legs of the switches [7]. Now let's assume that we take a single-phase full-wave CSI. So, the first switch 1 and 2 are ON. And here current will flow from the load and this current is positive. Now in the next sequence will turn OFF switch 1 and will switch ON switch 3 so that it could be short-circuited. So, the current will flow immediately from switches 3 and 2 and it has been short-circuited. But as the inductor will be connected with the DC source that's why the current will not increase much as the inductor will not allow the sudden change of current. Now in the case of the CSI, a diode is connected in series with the IGBT for that reason if the load becomes inductive then it will store some energy i.e., some of the energy is trapped in it. Now it has been seen that to release that inductive energy there is no path across the switches. So, the inductor voltage will keep on changing so the output current waveform remains constant but the voltage waveform changes. Although widely used when we talk about VSI, they have some limitations: (I) The AC output voltage is a certain amount lower than the source voltage (V_{in}). (II) At any point, the upper and the lower switches of any phase leg can't be turned ON, or else a short circuit can damage the switches. To protect this a dead time is in practice [1-3].

Here are some of the CSI limits: (I) The AC output voltage is higher than the source voltage. (II) At least one of the switches from the upper bank and the lower bank must be ON throughout

the time. Or else, the circuit will be open and high voltage spikes can damage the switches. To get rid of it an overlap time is preferred [7-8].

Impedance source or ZS network is a unique network by which power conversion between source and load in a wide range in an efficient way. In 2003 there was an evolution of a new type of converter which is called the Z-type converter [1]. And since then, this concept's research in power conversion applications [11] like AC-AC, DC-DC, AC-DC, and DC-AC has grown rapidly [12,16]. After that, the researchers proposed a new kind of pulse width modulation scheme specially for Z-source inverters (ZSI). And from there several medications and new-new topology of ZSI grew rapidly [1-3]. Now the limitations of the traditional inverter and a thorough comparison of traditional inverters and ZSI for the paper have been seen [4-8]. In 2004 there was a paper that discussed two of the controlled techniques that are used in ZSI [2-3]. The Maximum boost control (MBC) method [2] came in 2005, it has been observed that how the voltage stress across the switches can be minimized by using those methods. Although talking about Z-Source inverter, has several types [9-14] and these networks add positive values to the ZSI in certain ways [14-18]. In the Quasi Z-Source inverter, the two inductors are separated compared to the normal Z-Source inverter. Using this the voltage stress across the capacitors reduces thereby improving the input current profile [10]. Trans Z-Source inverter, two inductors are replaced by the transformer with a certain ratio. The input current is discontinuous here due to a different network structure [15]. Trans Quasi Z-Source inverters are certainly not in a use due to limitations. First, the input current is discontinuous with significant ripple, and the second is a large resonant [17] current at the starting. Active Quasi Z-Source inverter is used where significant voltage gain is the priority. And this is done by changing the shoot-through-duty ratio [18]. From the different papers, the different control method has been analysed. The various papers discussed the single-phase isolated ZSI [19]. The various paper discussed the space vector modulation technique in ZSI so that the PWM technique could be improved and become more efficient [19-22]. From there the research transferred from a two-level ZSI to a three-level ZSI with space vector modulation (SVM) [21]. As it has been observed from the papers that the MBC method is the most suitable for many applications because of voltage stress (V_s), the research is also going on to improve MBC and at the same time reduce the common-mode voltage switching patterns of a three-level ZSI [25]. Z-source can be used in many applications talking about renewable energy resources there is a various paper that shows wind energy [24,26] and a PV cell [27,34]. Although in these ZSIs,

one of the major challenges is reducing the inductor current Ripple [14]. Few of the papers describe how it can be reduced [28,35].

CHAPTER 3
RESEARCH GAP

It has been observed that for a ZSI there can be an establishment of a control algorithm so that the computational time reduces. Depending upon the desired output the ZSI will automatically calculate the appropriate modulation index and duty ratio. So, there will be a close loop system and that will make the ZSI more efficient i.e., it will function accurately based on the desired output voltage. For this computational time, different control algorithms have been compared and it has been founded that the event trigger method using sliding mode control is minimal. Based on the research gap, the following objectives are proposed.

1. Development of shoot-through insertion techniques for Z-Source inverter.
2. Analysis and comparison of different PWM techniques and topologies of Z-Source inverter.
3. Event trigger-based control algorithm for different PWM techniques.

CHAPTER 4
TOPOLOGIES OF ZSI

4. 1 Z-SOURCE INVERTER

ZS network or the impedance source network is a network that couples the main converters with the source. And this gives an energy-saving and effective way of power conversion between source and load. It actually differs significantly from voltage source and current source converters. One of the excellent and unique characteristics of the ZS network is that it may be operated as open-circuited and short-circuited as per the requirements, which was not possible with ordinary voltage sources and current source converters. And because of this again a unique characteristic comes out and that is it can serve as a step up and step down depending on the requirements. This Z-Source network is not limited only to the DC-AC converter but also can be used in various converters like DC-DC, AC-AC, and AC-DC. In the year 2002, this concept evolved. And from then till date modification and new Z- Source topologies have proliferated at an exponential rate. There are various types of ZSI they are, Quasi-ZSI followed by Trans-ZSI, Trans-Quasi-ZSI, and Active-Quasi-ZSI respectively. Each type of the ZSI has been discussed shortly with circuit diagrams.

4. 2 SCHEMATIC DIAGRAM OF Z-SOURCE INVERTER

Figure 4.1 shows the standard ZSI. ZS converter is a kind of power conversion scheme that uses passive components to buck and boost the input voltage. Actually, it connects the converter main circuit to the power supply using a distinct L-C impedance network, which allows it to enhance the input voltage, which is quite impossible with ordinary inverters. These are the two inductors L_1 and L_2 both are of the same values and size and two capacitors C_1 and C_2 are cross-coupled, to form a ZS. The six switches SW1, SW2, SW3, SW4, SW5, and SW6 respectively have been connected with SW1-SW4 in series, SW3-SW6, and SW5-SW2 with R-Phase, Y-Phase, B-Phase. From this circuit, it can be observed that a star-connected balanced resistance (R) load has been used. Also, a diode has been used in the circuit so that the current could not go to the supply side in any case, especially at the time of the shoot-through (ST) state. Another thing that can be observed from the circuit is that here sign of the capacitor should be kept in mind i.e., the positive side of the capacitor is connected to the $+ve$ side of the battery and the negative side of the capacitor is connected to the $-ve$ side of the battery.

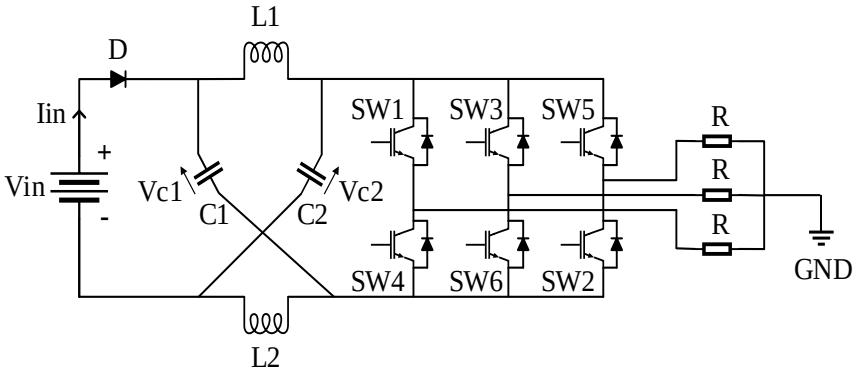

Figure 4. 1 Simple ZSI with resistive load

4. 3 QUASI Z-SOURCE INVERTER

Figure 4.2 shows the Quasi-ZSI (QZSI). This is almost the same as the ZSI i.e., a two-port network of LC circuit that couples the DC source side with the load side. Now the difference is that here two inductors are separated. Here the boost factor (B) is the same as the simple ZSI i.e.,

$$B = \frac{1}{1-2D_{st}} \tag{4.1}$$

where B is the boost factor and D_{st} is the ST duty ratio.

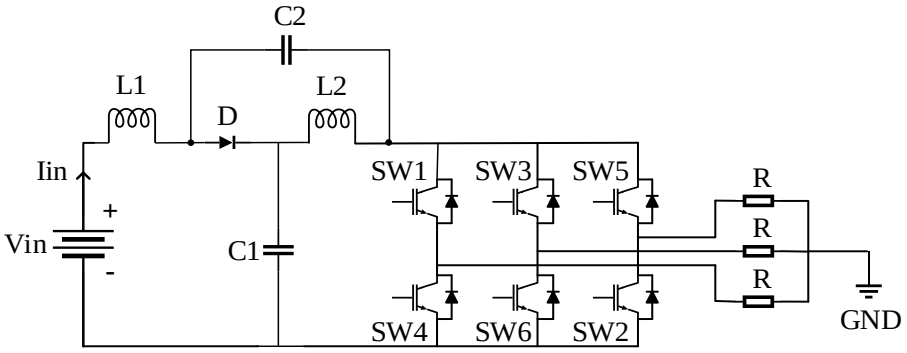

Figure 4. 2 Quasi ZSI with R load

The main advantage of the QZSI over a simple ZSI is that it maintains a lower V_s across the capacitors and thereby enhances the input current profile. QZSI is actually derived from traditional ZSI topology. There are some drawbacks of ZSI which actually overcome here.

4. 4 TRANS Z-SOURCE INVERTER

Figure 4.3 shows the voltage-fed Trans-ZSI (TZSI). Here it can be observed that two inductors that were used in the impedance network that has been replaced by a transformer with a ratio n: 1. The TZSI is also known as the T-source network. Here in this type of inverter as from Figure 4.3 it can be seen that the DC source is directly connected with the diode, that's why the current is discontinuous here in the case of boost mode.

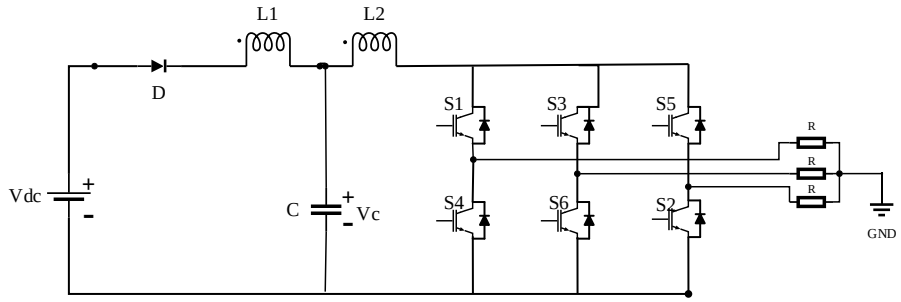

Figure 4. 3 Trans ZSI with resistive load

Now with this inverter, the B actually increases, and i.e., the B becomes,

$$B = \frac{1}{1-(1+n)\times\frac{T_{st}}{T}} = \frac{1}{1-(1+n)D_{st}} \tag{4.2}$$

4. 5 TRANS QUASI Z-SOURCE INVERTER

The Trans-Quasi-ZSI (TQZSI) has been depicted in Figure 4.4 and provides less voltage stress on the capacitor than that was there in the case of the TZSI. The source current in the case of the TQZSI is with major ripple as it actually flows to the bridge. Now, this is actually a limitation or restriction maybe for some applications, and to eliminate this issue, an LC filter is used at the front end of the circuit. Here also the B of the inverter increases and i.e.,

$$B = \frac{1}{1-(1+n)\times\frac{T_{st}}{T}} = \frac{1}{1-(1+n)D_{st}} \tag{4.3}$$

Here in all the above cases, n is the transformer's turn ratio.

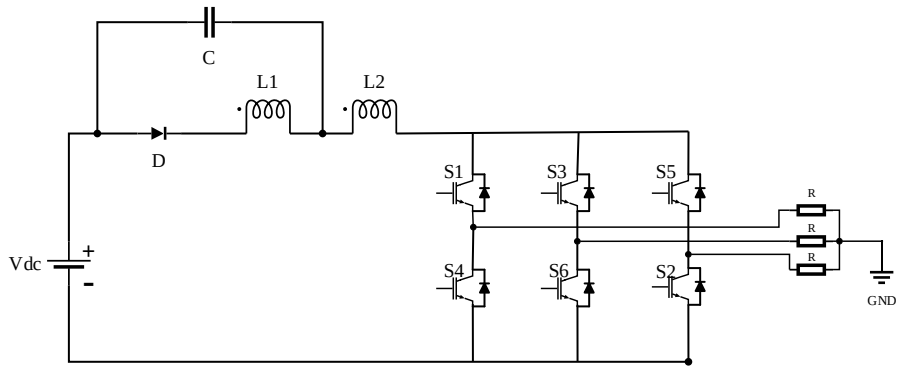

Figure 4. 4 Trans-Quasi ZSI with resistive load

Now if at any instant $n = 1$, both Trans-Z-source, as well as Trans-Quasi-Z-source, produce the output voltage gain as in the case of simple or traditional ZSI. Again, another possibility is there i.e., these inverters can get a strong boost inversion if $n > 1$. Although there is a typical Boost inversion enhancement but also these inverters have a number of drawbacks.

The first is that the TZSI's input DC current is discontinuous in nature whereas in the case of TZSI has a significant ripple in input DC current.

The second is that the TQZSI can subdue the resonant current at starting, but while talking about the TZSI. And that's why there is a spike of voltage and current resulting in damaging devices. So, the TQZSI is not having a start-up resonant problem but TZSI is having this problem because a large resonant current is actually traveling through the diode, transformer windings, capacitor, and IGBT (switches) body.

4. 6 ACTIVE QUASI Z-SOURCE INVERTER

The Active-Quasi-ZSI or AQZSI has been represented in Figure 4.5. The difference between the traditional ZSI and other above-mentioned ZSI, and this AQZSI is that this results in a significant voltage gain by altering the D_{st} and switching ratio n.

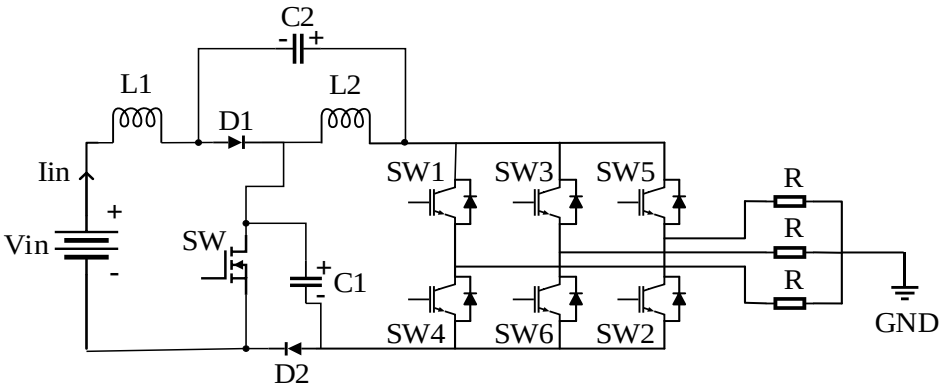

Figure 4. 5 Active-Quasi ZSI

Figure 4.2 shows the QZSI, now by modifying QZSI in Figure 4.5 with one or more switches and diodes with an enhanced PWM technique, the AQZSI in Figure 4.5 may provide a broader input voltage operating range.

CHAPTER 5
PWM TECHNIQUES OF ZSI

5.1 PULSE WIDTH MODULATION

PWM is a typical control technique by which we can generate analog signals from digital using various microcontrollers. Now hereafter closely observing the signals it can be observed that the signal is spread in a sequence of pulses in the PWM approach. By using the PWM approach, the variable voltage and the variable frequency can be achieved within the inverter and at the same time, a few lower-order harmonics can be eliminated. Now talking a little bit about the commutation, there are mainly two types of commutation one is natural commutation or line commutation and another one is force commutation. It is very obvious that in the PWM technique the force commutation is observable. Talking about pulse width modulation there are various types of PWM approaches that we use for voltage control inverters those are Single pulse-width modulation, Multiple pulse-width modulations, Sinusoidal pulse-width modulation (SPWM), Modified sinusoidal pulse-width modulation, and Phase-displacement control. Among all of these only SPWM has been used along with one unique state called the ST state. Here in the case of our circuit, we have used three distinct PWM techniques with different salient features. These are the SBC Method, MBC, and MCBC Control Method. These methods will be discussed further below thoroughly.

5.2 SIMPLE BOOST CONTROL METHOD

SPWM is a traditional PWM technique i.e., by comparing the sine wave and triangular wave whatever pulse we are getting that is there in this method for six active states. But also, this is a unique method as inserting ST is different. In this method, ST is injected into all the PWM zero states for a full cycle.

The two constant lines, one is $+ve$ and one $-ve$ in Figure 5.1 was used to understand the ST ratio (D_{st}). Whatever the amplitude of the three-phase voltage, the same amplitude is chosen for the constant lines with alternate signs discussed above.

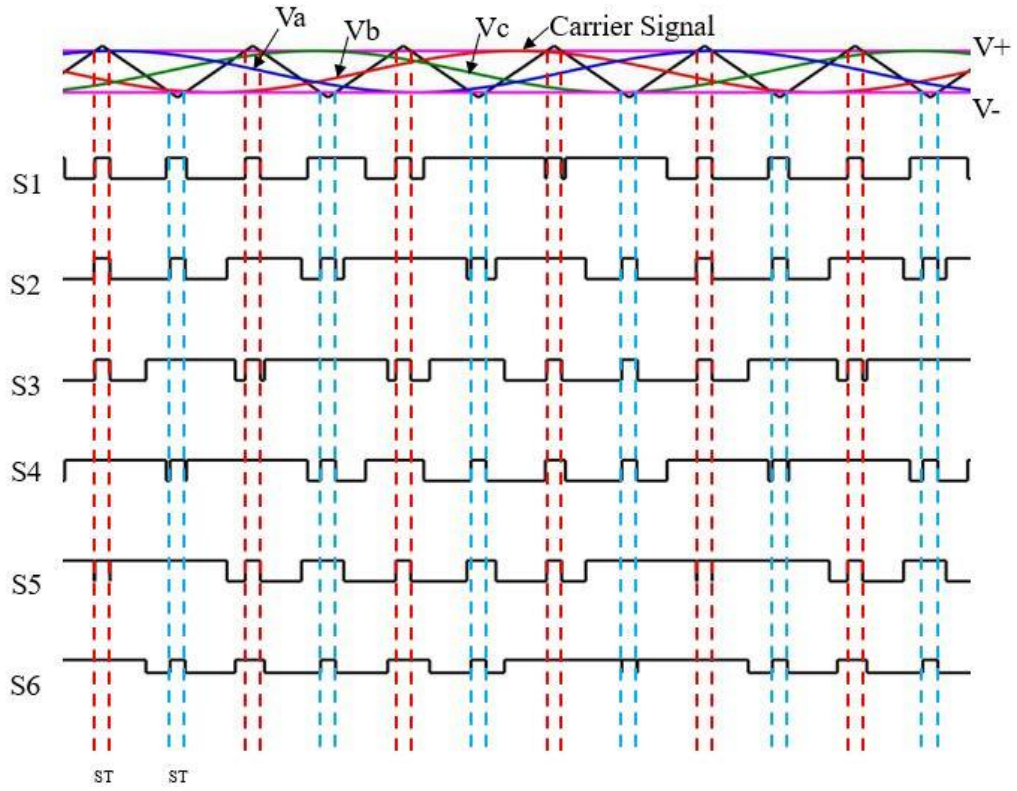

Figure 5. 1 Representation of SBC Method

At any instant, the triangular wave is more than the $+ve$ constant line, and vice-versa the for the $-ve$ constant line the ST will take place.

5.3 MAXIMUM CONSTANT BOOST CONTROL METHOD

By maintaining the duty ratio constant this method helps to maximize the voltage gain (G). MCBC method is represented in Figure 5.2. SPWM is as it is as like as SBC i.e., for six active states. The injection process of ST is very much different here compare to SBC which makes it unique. For adding ST two envelopes one $+ve$ and another $-ve$ has been created over here. And that has been shown in Figure 5.2, $V_+ \; and \; V_-$.

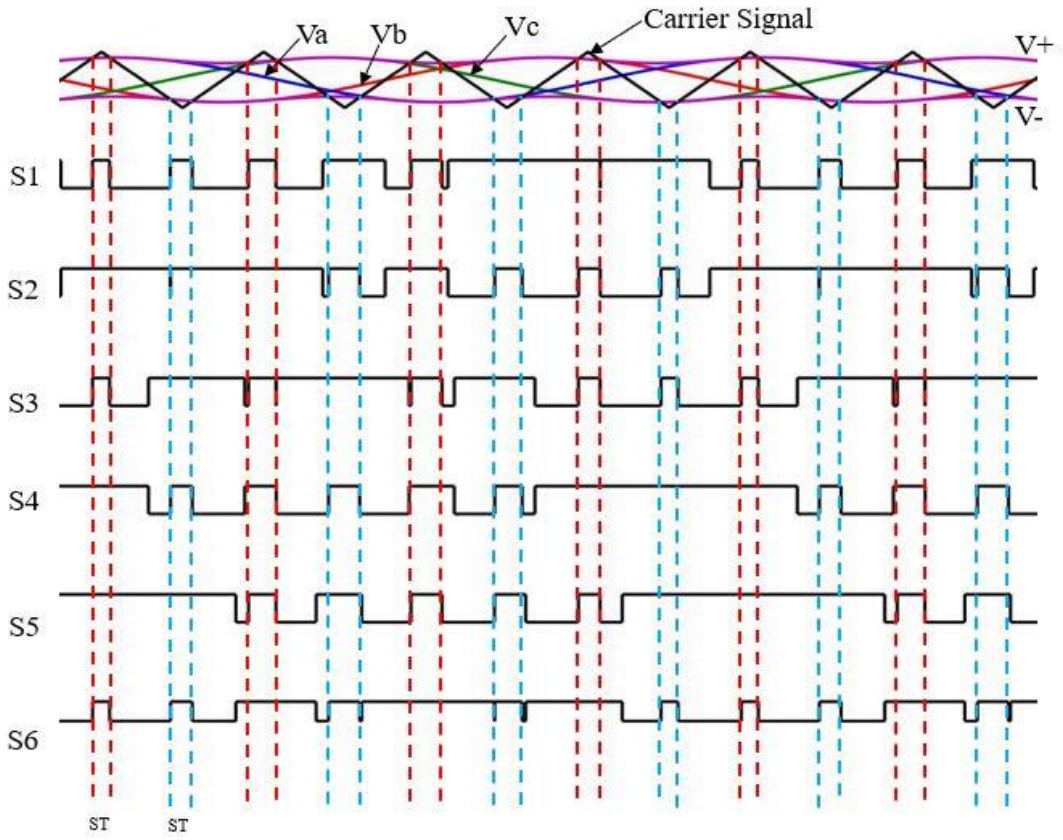

Figure 5. 2 Representation of MCBC Method

Both the envelopes are periodical and its frequency is 3 times the fundamental frequency of sinusoidal reference signal. Here our output f is $50\ Hz$ so the both the envelopes f wolud be $150\ Hz$ to valid the ST injection. And it is switched up and down based on the modulation index (M). Now at any instant the triangular wave is more than the V_+ and vice-versa the for the V_- the ST will take place.

5.4 MAXIMUM BOOST CONTROL METHOD

This control method is very much similar to the SPWM technique with a slight difference in the ST injection process. Figure 5.3 illustrates the ST injection process for MBC.

From Figure 5.3, we can see that ST occurs at any moment the triangular wave is more w.r.t $V_a, V_b\ and\ V_c$ and vice versa. Here we need to see which of the three waveforms is a bit more $+ve$ and at the same time which is a bit $-ve$ on any occasion. And we need to give ST accordingly. Here rather than being consistent throughout the cycle, ST changes from cycle to cycle.

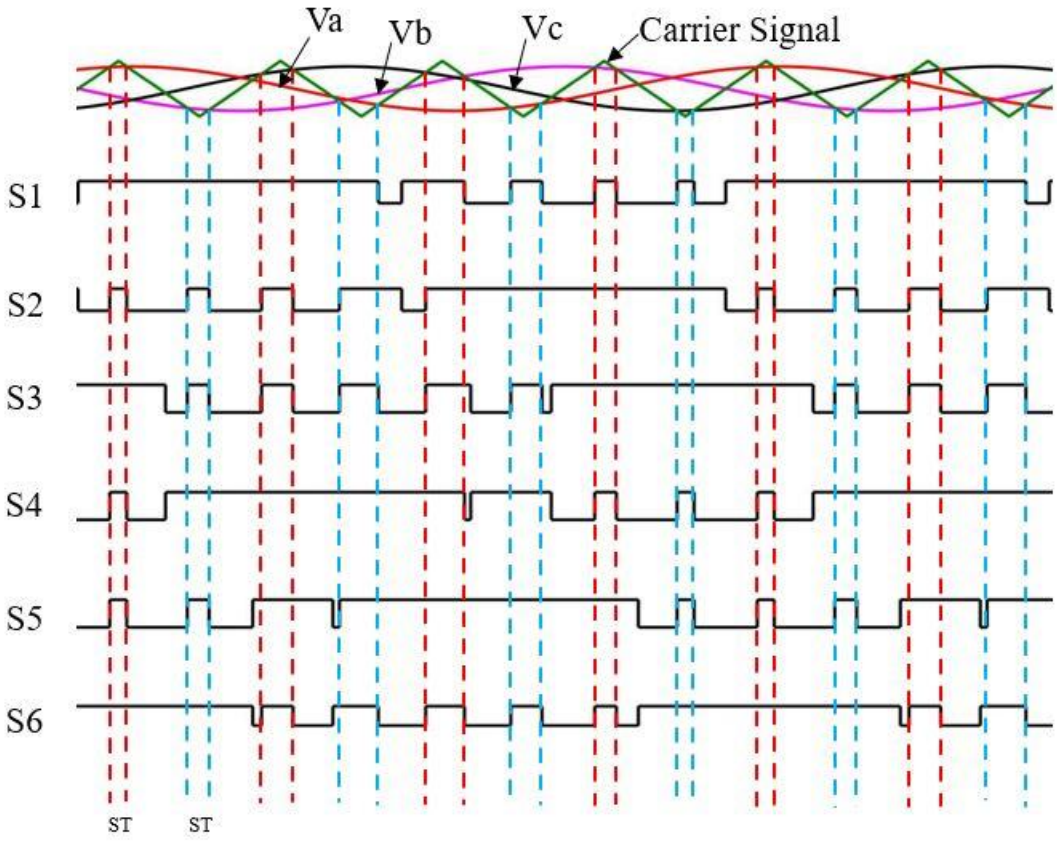

Figure 5. 3 Representation of MBC Method

5.5 SPACE VECTOR MODULATION TECHNIQUE

To supply variable voltage and f for drives, a three-phase VSI is always employed. A number of PWM techniques have been reported to get variable voltage and f supply. The most common ones are carrier-based sinusoidal PWM and space vector pulse width modulation (SVPWM). This carrier-based sinusoidal PWM technique has one major disadvantage is lower DC bus utilization. The introduction of space vector modulation improves DC bus utilization by 15.15% and further digital implementation of this scheme is easier. SVM is one of the most popular real-time modulation algorithms, and it's commonly utilized for digital control of VSIs. Revolving MMF in 3-Φ machines is an example of SVM.

In the inverter how the switches are operating can be represented by switching states in Table I. Here switching state ‘1’ denotes that one of the upper switches of the inverter leg is on while ‘0’ indicates that one of the lower switches of the inverter leg is on.

TABLE 5. 1 Different switching states with conducting switches

Switching States	Conducting Switches
100	S1, S6, S2
110	S1, S3, S2
010	S4, S3, S2
011	S4, S3, S5
001	S4, S6, S5
101	S1, S6, S5
111	S1, S3, S5
000	S4, S6, S2

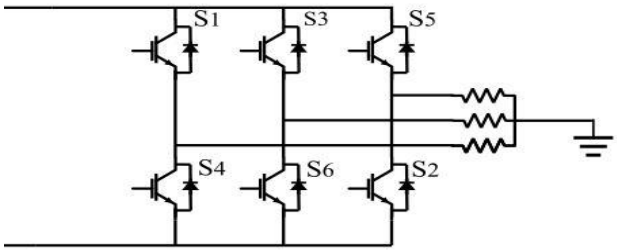

Figure 5. 4 3-Φ inverter circuit with 6 switches

As Figure 5.4. in the 3-Φ inverter there are 6 switches, and there are 8 different combinations i.e., 8 different states of the inverter. So, the inverter produces 8 states of output voltages. The switching state (100), for example, corresponds to the conduction of S1, S6, and S2 in the inverter legs respectively. So, in those 8 states, 6 are the active states or non-zero states and 2 are zero states. The 2 zero states are (111) and (000) when all the upper and all the lower switches are in conduction.

Now there is 3-Φ winding and this essentially produces a rotating magnetomotive field (mmf). It can also be done by 2-Φ winding one will be called α and another is β. Like Figure 5.5**.** this α and β are 90˚ apart from each other. This can also be excited by the current phase shifted by 90˚ in time. And by this, a revolving mmf can be produced. So, for 3-Φ winding an equivalent 2-Φ winding can be considered. The idea can be extended for 3-Φ voltage in a similar manner.

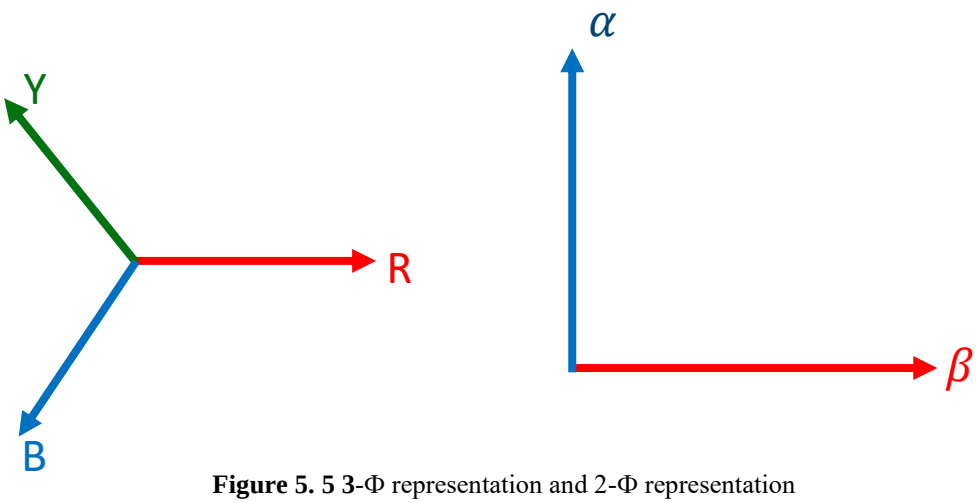

Figure 5. 5 3-Φ representation and 2-Φ representation

A space vector diagram for a two-level inverter is shown below. In Figure 5.6 (0) and (7) is called zero state. These two are called zero states because there is no transfer of power between the DC side and AC side. Other states from (1 – 6) are called active states because during this state there is a transfer of power between the DC side and AC side. The active and zero switching states can be represented by active and zero space vectors, respectively. So, with six active vectors, there will be 6 sectors with 6 active vectors $\overrightarrow{V1}$ to $\overrightarrow{V6}$ and the zero vector $\overrightarrow{V0}$ and $\overrightarrow{V7}$ lies at the center.

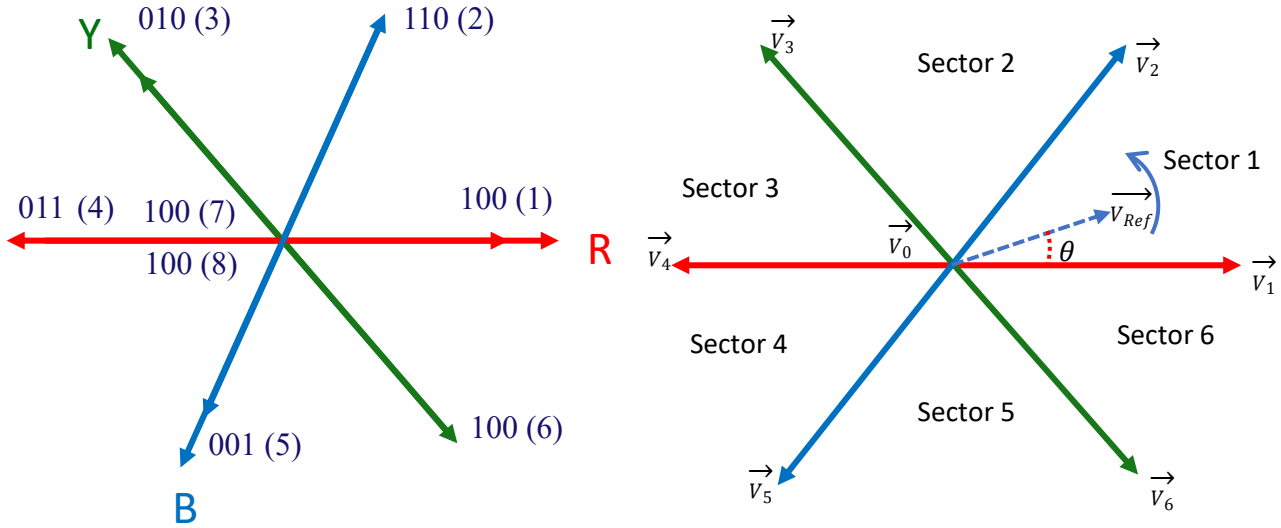

Figure 5. 6 Space Vector diagram for two-level inverters

So, from Figure 5.6. it can be concluded that if we need to find $\overrightarrow{VRef}$ then it can be found by using parallelogram law as $\overrightarrow{V1}$ and $\overrightarrow{V2}$ is known.

Phase-to-neutral voltages of a star-connected load can be found by a voltage difference of star point neutral i.e., N and DC negative rail N.

$$Va = VA - VnN \tag{5.1}$$

$$Vb = VB - VnN,\ Vc = VC - VnN \tag{5.2}$$

It has been seen that the phase voltages in a star-connected load sum to zero so,

$$V_a + V_b + V_c = 0 \tag{5.3}$$

Putting the (5.1) and (5.2) in the (5.3),

$$VnN = \frac{1}{3}(VA + VB + VC) \tag{5.4}$$

Again, putting (5.4) in (5.1) and (5.2),

$$Va = \frac{2}{3}VA - \frac{1}{3}(VB + VC) \tag{5.5}$$

$$Vb = \frac{2}{3}VB - \frac{1}{3}(VA + VC)\ and \quad Vc = \frac{2}{3}VC - \frac{1}{3}(VB + VA) \tag{5.6}$$

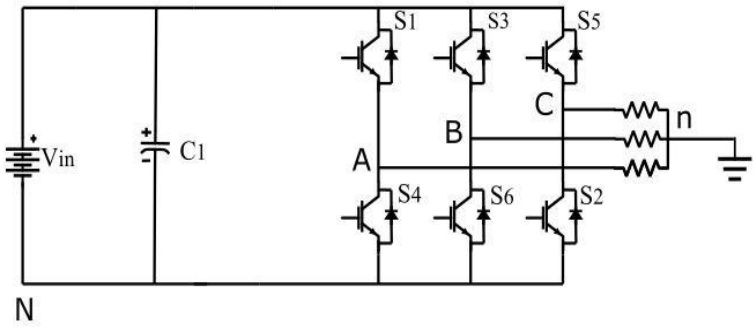

Figure 5. 7 3-Φ VSI circuit diagram

TABLE 5. 2 Magnitude of phase voltage values at different switching states

State	Switches on	VA	VB	VC
1	100	$^{2}/_{3}$ Vin	$^{-1}/_{3}$ Vin	$^{-1}/_{3}$ Vin
2	110	$^{1}/_{3}$ Vin	$^{1}/_{3}$ Vin	$-\,^{2}/_{3}$ Vin
3	010	$^{-1}/_{3}$ Vin	$^{2}/_{3}$ Vin	$^{-1}/_{3}$ Vin
4	011	$-\,^{2}/_{3}$ Vin	$^{1}/_{3}$ Vin	$^{1}/_{3}$ Vin
5	001	$^{-1}/_{3}$ Vin	$^{-1}/_{3}$ Vin	$^{2}/_{3}$ Vin
6	101	$^{1}/_{3}$ Vin	$-\,^{2}/_{3}$ Vin	$^{1}/_{3}$ Vin
7	111	0	0	0

8	000	0	0	0

By the equations (5.5) and (5.6) it can be cleared that various switching states will get the different magnitudes of phase voltages and that has been shown in Table 5.2.

CHAPTER 6

ANALYSIS OF DIFFERENT TOPOLOGIES AND PWM TECHNIQUES

6.1 MATHEMATICAL DERIVATIONS

6.1.1 Z-SOURCE INVERTER DERIVATIONS

There are two states one is ST and another is NST (Non-ST). This NST is also called an active state. Figure 6.3 represent the ST i.e., similar to short-circuited, and Figure 6.2 illustrates the NST where the power is actually traveling from the source side to the load side.

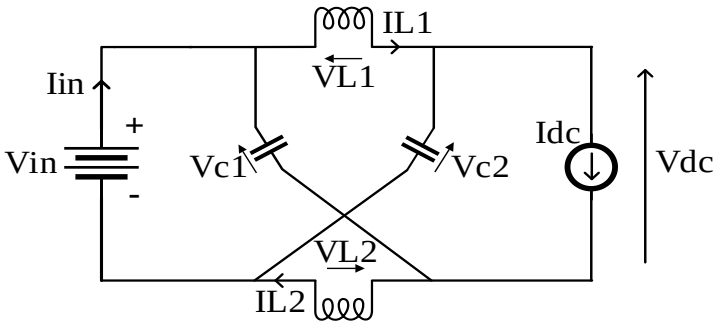

Figure 6. 1 ZSI equivalent circuit representation

Figure 6.1 illustrate the ZSI equivalent circuit where L_1 and L_2 are of equal magnitude and the same for C_1 and C_2. Because of Identical values, the ZS network becomes exactly symmetrical in nature. So, it can be said that,

$$V_{c1} = V_{c2} = V_c \tag{6.1}$$

$$V_{l1} = V_{l2} = V_l \tag{6.2}$$

Considering Figure 6.3 where ST is happening for a time T_{st} and total time is T. From this state we have,

$$V_l = V_c \tag{6.3}$$

$$V_{dc} = 0 \tag{6.4}$$

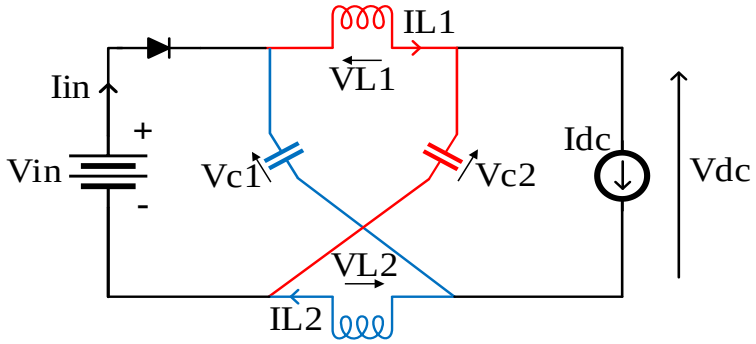

Figure 6. 2 ZSI at NST representation

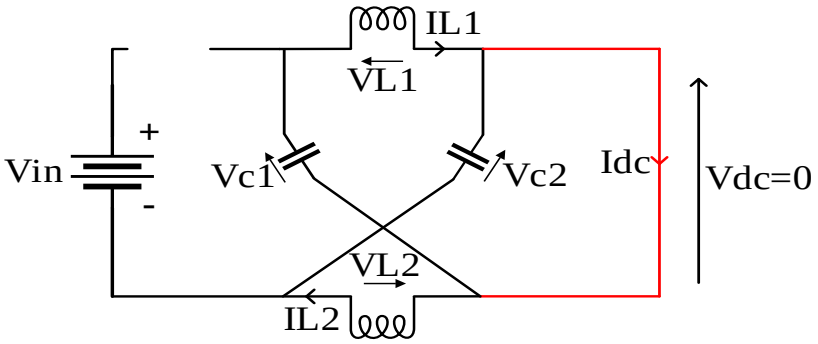

Figure 6. 3 ZSI at ST representation

Now taking consider Figure 6.2 i.e., the NST state which is occurring over time T_a. It can be clearly observed from Figure 6.1 that,

$$V_l = V_{in} - V_c \tag{6.5}$$

$$V_{dc} = V_c - V_l \tag{6.6}$$

Now, substituting (6.5) in equation (6.6) one has,

$$V_{dc} = 2V_c - V_{in} \tag{6.7}$$

$$V_{l(avg)} = \frac{T_{st} \cdot V_c + T_a \cdot (V_{in} - V_c)}{T} \tag{6.8}$$

Setting the equation (6.8) to zero in S.S. gives,

$$V_C = \frac{T_a}{T_a - T_{st}} \cdot V_{in} \tag{6.9}$$

Similarly for DC link voltage,

$$V_{dc_{avg}} = \frac{T_{st} \cdot 0 + T_a \cdot (2V_c - V_{in})}{T}$$

$$= \frac{T_a}{T_a - T_{st}} V_{in} = V_c \tag{6.10}$$

By substituting (6.9) into equation (6.7), $V_{dc}\ peak$ can be determined.

$$V_{dc} = \frac{T}{T_a - T_{st}} V_{in} \tag{6.11}$$

$$V_{dc(peak)} = B.V_{in} \tag{6.12}$$

Where B is,

$$B = \frac{T}{T_a - T_{st}} \tag{6.13}$$

$$B = \frac{1}{1 - 2\frac{T_{st}}{T}} \tag{6.14}$$

The $V_{ac}\ peak$ of a conventional VSI is given as,

$$V_{ac(Peak)} = 0.5 \times V_{dc(peak)} \times \frac{V_{ref}}{V_{car}} \tag{6.15}$$

$$V_{ac_{peak}} = M \times \frac{V_{dc(peak)}}{2} \tag{6.16}$$

From equations (6.12) and (6.16) a new output ac voltage peak can be obtained for ZSI.

$$V_{ac(Peak)} = M \times B \times \frac{V_{in}}{2} \tag{6.17}$$

From (6.1), (6.9), and (6.14) the capacitor voltage can be obtained

$$V_{c1} = V_{c2} = V = \frac{\frac{T_a}{T}}{\frac{T_a}{T} - \frac{T_{st}}{T}} \cdot V_{in} \tag{6.18}$$

$$\text{As, } T = T_a + T_{st} \tag{6.19}$$

Putting (6.19) in (6.18) we have,

$$V_c = \frac{1-\frac{T_{st}}{T}}{1-\frac{2 \cdot T_{st}}{T}} \cdot V_{in} \tag{6.20}$$

For T_{st} the ST arises. B is the foremost thing, it can be observed from equation (6.17) how B is dependent on $V_{ac}\ peak$. Also T_{st} performs valid over here. As there is an increase in T_{st}, B increases, and that is reflected on $V_{ac}\ peak$ and vice versa.

6.1.2 QUASI Z-SOURCE INVERTER DERIVATION

Figure 6.4 shows the QZSI. Now talking about the QZSI, it has two types of operational states like the classic ZSI. One is the NST state and another is the ST state. When seen from the DC side, the inverter bridge is comparable to a current source in NST states.

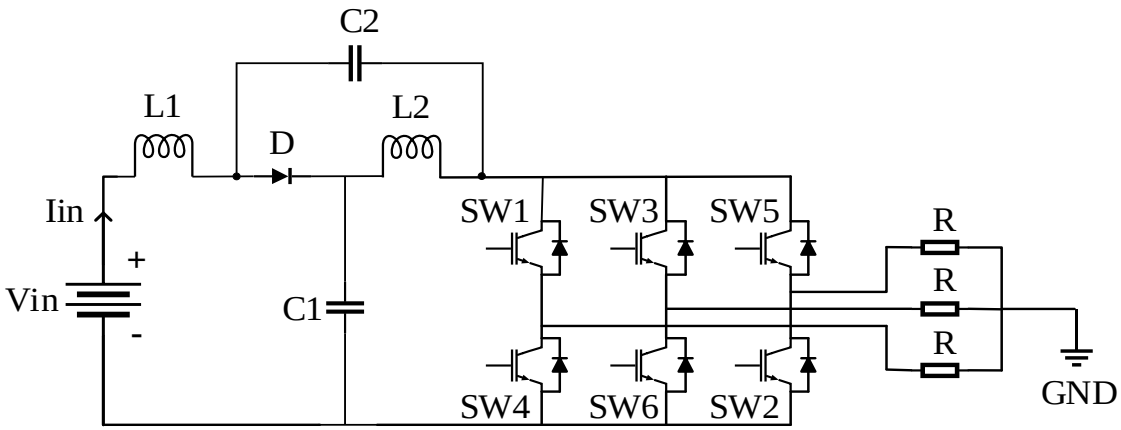

Figure 6. 4 Simple QZSI circuit representation with R load

Figure 6.5 and Figure 6.6 illustrate the analogous circuits for the two states. Talking about the classic VSI the ST state is prohibited since it will be short-circuited and may damage the switches. Here also like the traditional ZSI the unique LC and diode network i.e., coupled to the inverter bridge modifies the behaviour of the circuit and thereby permits the shoot condition.

When the ST happens, this network successfully protects the circuit, and the QZSI enhances the DC-link voltage by leveraging the ST condition. As ZSI has been discussed in the above topics, it can be noted that there is a difference between the ZSI and QZSI i.e., in the case of the ZSI, the impedance network draws the discontinuous current but when talking about the QZSI, it draws continuous constant DC current from the source. The second thing is that here in the case of QZSI the capacitor C_2 voltage is considerably lowered.

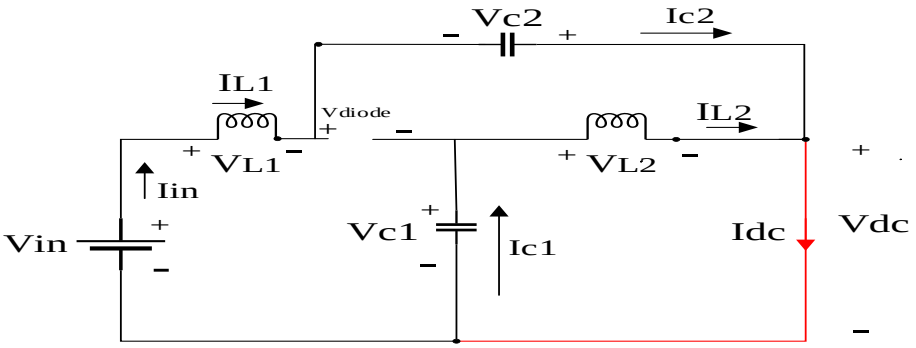

Figure 6. 5 QZSI at ST representation

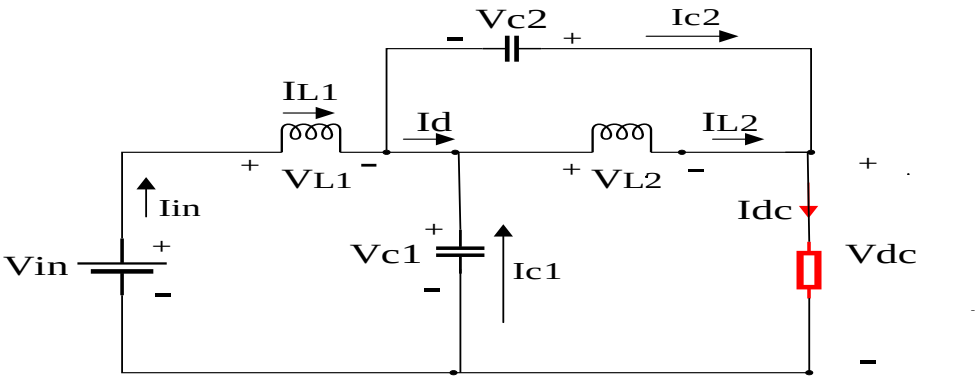

Figure 6. 6 QZSI at NST representation

All the current with directions and voltage with the polarity has been shown in Figure 6.5 and Figure 6.6 respectively.

Here also total time (T) i.e., $T = T_{st} + T_a$ as like the ZSI.

Where T_{st} is ST time, whereas T_a is NST time. As like the ZSI the duty ratio (D_{st}) is

$$D_{st} = \frac{T_{st}}{T} \tag{6.21}$$

First for the ST state, considering Figure 6.5 where shoot-through is happening for a time T_{st}. From this state we have,

$$V_{dc} = 0 \tag{6.22}$$

$$V_{diode} = V_{C1} + V_{C2} \tag{6.23}$$

$$V_{L1} = V_{C2} + V_{in} \quad and \quad V_{L2} = V_{C1} \tag{6.24}$$

Now taking consider Figure 6.6 i.e., the NST state which is occurring over time T_a.

$$V_{diode} = 0, \text{ here diode is forward bias} \tag{6.25}$$

$$V_{L1} = V_{in} - V_{C1} \tag{6.26}$$

$$V_{L2} = -V_{C2}, \text{ and} \tag{6.27}$$

Talking about the DC link voltage,

$$V_{dc} = V_{C1} - V_{L2} = V_{C1} + V_{C2} \tag{6.28}$$

Now talking about the average voltage of the inductor from (6.24), (6.26), and (6.27) it can be stated that,

$$V_{L1_{avg}} = \frac{T_{st}(V_{C2}+V_{in})+T_a(V_{in}-V_{C1})}{T} = 0 \tag{6.29}$$

And for L_2 it can be stated as,

$$V_{L2_{avg}} = \frac{T_{st}(V_{C1})+T_a(-V_{C2})}{T} = 0 \tag{6.30}$$

After solving the above equation, one has,

$$V_{C1} = \frac{T_a}{T_a - T_{st}} V_{in}, \quad and \quad V_{C2} = \frac{T_{st}}{T_a - T_{st}} V_{in} \tag{6.31}$$

From (6.25), (6.28), (6.22), (6.23), and (6.31) the average DC link voltage across the inverter bridge is,

$$V_{dc} = V_{C1} + V_{C2} = \frac{T}{T_a - T_{st}} V_{in} = \frac{1}{1-2\frac{T_{st}}{T}} V_{in} = BV_{in} \tag{6.32}$$

As like in the ZSI here also B is the boost factor. Here V_{dc} is again the peak voltage across the diode.

Now across the L_1 and L_2 the average current will be,

$$I_{L1} = I_{L2} = I_{in} = P/V_{in} \tag{6.33}$$

Here P is the power of the entire system

Now, current across the capacitors can be written as, according to the KCL and equation number (6.12) i.e.,

$$I_{C1} = I_{C2} = I_{dc} - I_{L1} \tag{6.34}$$

$$I_{diode} = 2I_{L1} - I_{dc} \tag{6.35}$$

Talking about the QZSI there are many advantages that actually derive from ZSI. With a particular B, it may buck or boost the voltage. It is more dependable than the classical VSI since it can manage an ST state. In addition, when compared to the ZSI, the QZSI has certain distinct advantages. They are, in ZSI, the two capacitors maintain the same high voltage, whereas, in QZSI, the voltage across the capacitor $C2$ is reduced, so it is possible to use a lower capacitor rating. Second thing is that the input current of the ZSI is discontinuous in boost mode, but the input current of the QZSI is continuous owing to input inductor $L1$, reducing the input stress. And last is that talking about the QZSI, between the source and the inverter there is a single DC rail, which makes assembly easier and reduces EMI.

6.1.3 SIMPLE BOOST CONTROL METHOD DERIVATION

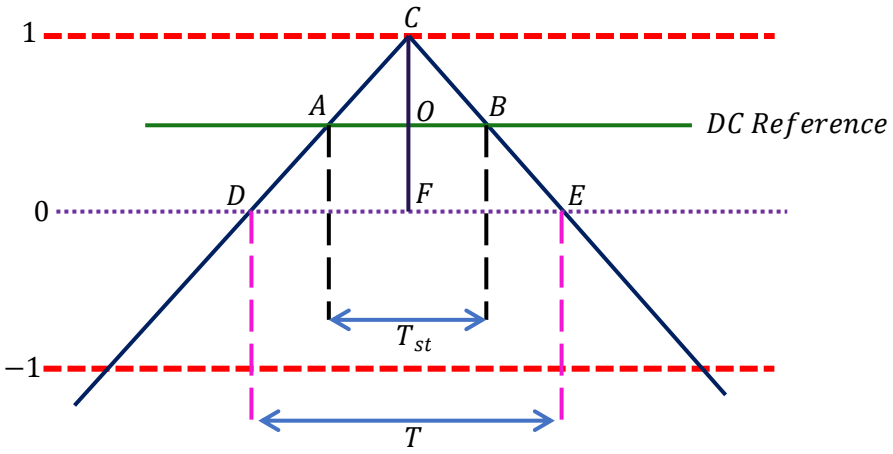

Figure 6. 7 Comparison of DC line with a triangular wave to justify D_{st} and M relationship

ΔABC is symmetrical to ΔDEC ,

$$\text{Now} \quad AB = T_{st},\ DE = T,\ CF = AC$$

$$\frac{AB}{DE} = \frac{CO}{CF} = \frac{CF - OF}{CF}$$

$$\frac{T_{st}}{T} = \frac{AC_{Peak} - A_{ref_{Peak}}}{AC_{Peak}}$$

$$\frac{T_{st}}{T} = \frac{AC_{Peak}}{AC_{peak}} - \frac{A_{ref_{Peak}}}{AC_{Peak}}$$

$$\frac{T_{st}}{T} = 1 - M$$

$$D_{st} = \frac{T_{st}}{T} = 1 - M \tag{6.36}$$

So, it can say that the maximum ST duty ratio D_{st} is limited to $(1 - M)$ in the case of SBC. So, as M reaches one, the M becomes zero and B becomes one in that case.

The G of each system is calculated as follows,

$$G = \frac{V_{out}}{V_{in}} \tag{6.37}$$

$$G = \frac{V_{ac(peak)}}{V_{in}/2} \tag{6.38}$$

From equation (6.17), one has

$$\frac{V_{ac(Peak)}}{V_{in}/2} = MB = G \tag{6.39}$$

Relationship between $G, M,$ and D_{st} can be obtained by putting equation (6.14) in equation (6.39)

$$G = M \times \frac{1}{1-D_{st}} \tag{6.40}$$

$$G = \frac{M}{2M-1} \qquad \therefore D_{st} = 1 - M \tag{6.41}$$

V_{dc} is nothing but Voltage Stress (V_s) over the switches. It can be written from equation (6.12)

$$V_s = B \cdot V_{in} \tag{6.42}$$

It is seen that as M reduces the ST duty ratio shoots up. Since overall interval time T is fixed so, as D_{st} shoots up T_{st} also, rise i.e., form equation (6.14) B also shoots up and finally V_s rises.

From equations (6.39) and (6.42)

$$V_s = G\frac{V_{in}}{M} \tag{6.43}$$

Putting $D_{st} = 1 - M$ in (6.14) we get,

$$B = \frac{1}{2M-1} \tag{6.44}$$

Substituting (6.44) into (6.42)

$$V_s = \frac{V_{in}}{2M-1} \tag{6.45}$$

Therefore, for vital G the largest possible M can be obtained from equation (6.41)

$$M = \frac{G}{2G-1} \tag{6.46}$$

Through equations (6.42), (6.43), and (6.44) V_s can be obtained as

$$V_s = (2G-1)V_{in} \tag{6.47}$$

6.1.4 MAXIMUM BOOST CONTROL METHOD DERIVATION

Let's consider a switching time interval from $\frac{\pi}{6}$ to $\frac{\pi}{3}$ i.e., to find out the average duty ratio by integrating $\frac{T_{st}}{T}$ with respect to angle $d\theta$.

$$\frac{T_{st}}{T}(avg) = \int_{\frac{\pi}{6}}^{\frac{\pi}{2}} \frac{2-\left(Msin\theta - Msin\left(\theta-\frac{2\pi}{3}\right)\right)}{2} d\theta$$

$$\frac{T_{st}}{T}(avg) = \frac{2\pi-3\sqrt{3}M}{2\pi} \tag{6.48}$$

Substituting equation (6.48) in equation (6.14), one can get

$$B = \frac{\pi}{3\sqrt{3}M-\pi} \tag{6.49}$$

We know,

$$G = \frac{V_{out}}{V_{in}} \tag{6.50}$$

$$G = \frac{V_{ac(peak)}}{V_{in}/2} \tag{6.51}$$

From equation (6.17)

$$\frac{V_{ac(Peak)}}{V_{in}/2} = M \times B = G \tag{6.52}$$

Relationship between $G, M, and\ D_{st}$ is obtained by Putting equation (6.14) in (6.52),

$$G = M \times \frac{1}{1-D_{st}} \tag{6.53}$$

$$G = \frac{\pi M}{3\sqrt{3}M-\pi} V_{dc} \tag{6.54}$$

is actually the Stress across the switch during OFF condition. So, From equation (6.12)

$$V_s = B \cdot V_{in} \tag{6.55}$$

From equations (6.52) and (6.55)

$$V_s = G \frac{V_{in}}{M} \tag{6.56}$$

Putting (6.48) in (6.14)

$$B = \frac{\pi}{3\sqrt{3}M-\pi} \tag{6.57}$$

After Putting (6.57) in (6.55) we get a relation of V_s in terms of $M$and DC input voltage.

$$V_s = \frac{V_{in}\times\pi}{3\sqrt{3}M-\pi} \tag{6.58}$$

So, for required G the possible M is written as from (6.54) is,

$$M = \frac{\pi G}{3\sqrt{3}G-\pi} \tag{6.59}$$

From (6.55), (6.56), and (6.59) we can get the V_s in this MBC,

$$V_s = \frac{3\sqrt{3}G-\pi}{\pi} V_{in} \tag{6.60}$$

6.1.5 MAXIMUM CONSTANT BOOST CONTROL METHOD DERIVATION

Assuming that the first half cycle is 0 to $\frac{\pi}{3}$ so, the top and bottom envelopes during this cycle can be expressed as,

$$V_{+1} = \sqrt{3}M + Msin\left(\theta - \frac{2\pi}{3}\right) \tag{6.61}$$

and

$$V_{-1} = Msin\left(\theta - \frac{2\pi}{3}\right) \quad (6.62)$$

And for next $\frac{\pi}{3}$ to $\frac{2\pi}{3}$ the upper and lower envelope curves can be expressed in the equation

$$V_{+2} = Msin(\theta) \quad (6.63)$$

and

$$V_{-2} = Msin(\theta) - \sqrt{3}M \quad (6.64)$$

From these two equations, we can see that deducting equation (6.62) from (6.61) yields $\sqrt{3}M$ i.e., the interval between two envelopes.

We know G can be written as

$$G = \frac{V_{out}}{V_{in}} \quad (6.65)$$

$$G = \frac{V_{ac(peak)}}{V_{in}/2} \quad (6.66)$$

From equation (6.17) one has

$$\frac{V_{ac(Peak)}}{V_{in}/2} = M \times B = G \quad (6.67)$$

$$\frac{T_{st}}{T} = D_{st} = \frac{2-\sqrt{3}M}{2} = 1 - \frac{\sqrt{3}M}{2} \quad (6.68)$$

The relationship among $G, M, and\ D_{st}$ can be acquired by substituting equation (6.14) into (6.67)

$$G = M \times \frac{1}{1-D_{st}} \quad (6.69)$$

$$G = \frac{M}{\sqrt{3}M-1} \quad (6.70)$$

Now here in equation (6.70) as soon as M reaches to $\frac{\sqrt{3}}{3}$ the G becomes infinity.

DC link voltage V_{dc} is actually the V_s across the switch during the OFF condition of the switch. So, From equation (6.12)

$$V_s = B \cdot V_{in} \tag{6.71}$$

From equations (6.67) and (6.57)

$$V_s = G \frac{V_{in}}{M} \tag{6.72}$$

Putting (6.68) in (6.14)

$$B = \frac{1}{\sqrt{3}M-1} \tag{6.73}$$

substituting (6.73) in (6.71), we get a relation among V_s in terms of M and V_{in}.

$$V_s = \frac{V_{in}}{\sqrt{3}M-1} \tag{6.74}$$

Therefore, for vital G, the feasible M can be said from equation (6.70) i.e.,

$$M = \frac{G}{\sqrt{3}G-1} \tag{6.75}$$

V_s can be acquired from equations (6.71), (6.72), and (6.75)

$$V_s = \left(\sqrt{3}G - 1\right)V_{in} \tag{6.76}$$

6.2 COMPARISONS

As discussed above talking about comparison, there are many methods like SBC, MBC, and MCBC. These are different pulse width modulation methods that have been used here. All PWM are distinct from each other and often have some advantages and disadvantages over one another.

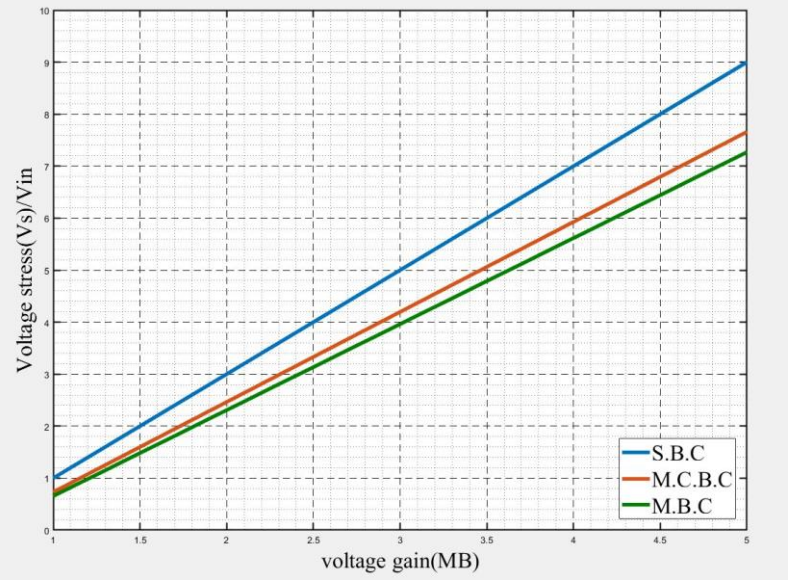

Figure 6. 8 Voltage gain (MB) vs V_s / V_{in}

In Figure 6.8 the G Vs V_s / V_{in} graphs have been expressed with all three approaches SBC, MCBC, and MBC. Figure 6.8 can be used to survey about the V_s of various modulation approaches. It can be noticed that the SBC method acquires a big V_s over others. Furthermore, MBC acquires minimum V_s among all. Talking about V_s it is the foremost thing because the grade of the switches relies on it.

Figure 6.9, express the D_{st} with reference to G. By this, it has been noted that along with a rise in D_{st}, maximal G is observed with SBC, MCBC, and MBC respectively.

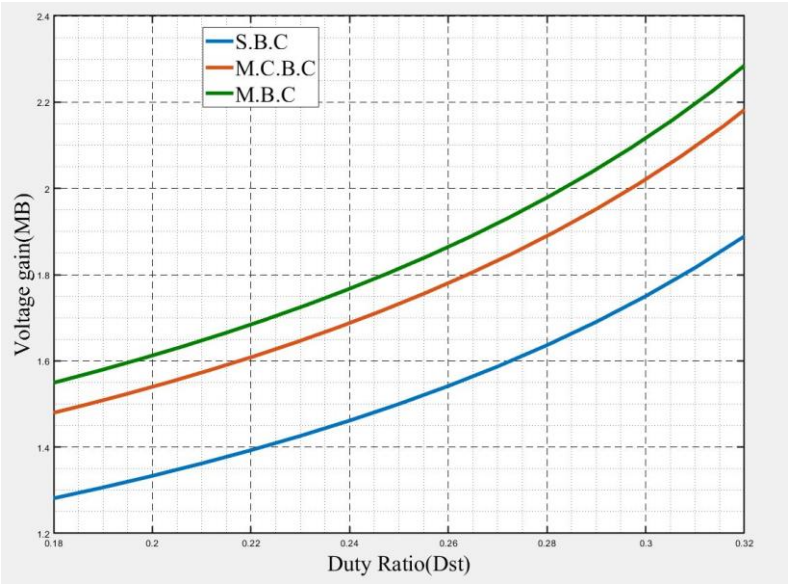

Figure 6. 9 Duty Ratio (D_{st}) Vs Voltage Gain (MB)

A chart of G Vs M has been shown in Figure 6.10 with SBC, MCBC, and MBC respectively. From this Figure 6.10, we can see that the operating range expands as M shoots up. SBC is with maximum operating area followed by MCBC and MBC respectively.

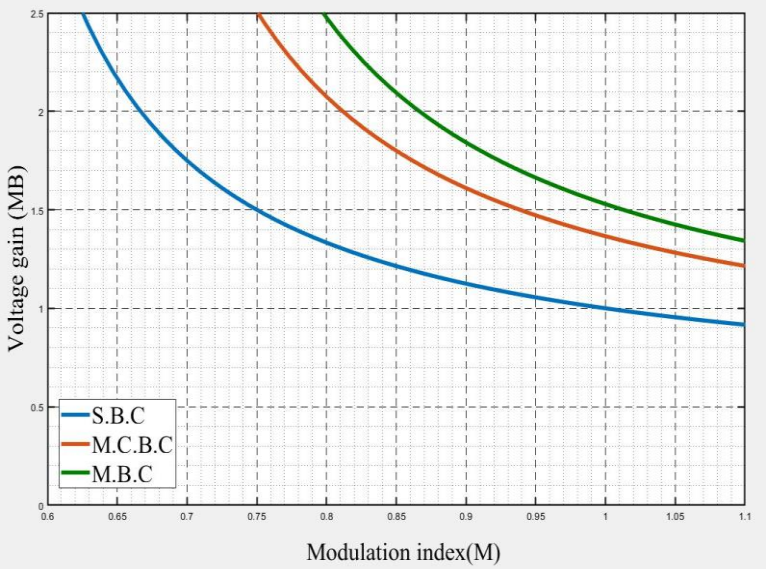

Figure 6. 10 Modulation Index (M) Vs Voltage gain (MB)

TABLE 6. 1 With a constant gain $G = 1.7$ different control methods comparisons

PARAMETERS	**SBC**	**MCBC**	**MBC**
M	0.7083	0.8742	0.9382
ΔI_L	13.83 A	13.38 A	24.56 A
B	2.4	1.945	1.812
V_S (SW) Peak	310.6 V	241.9 V	252.3 V
V_L Peak	219.0 V	182.5 V	222.1 V
V_{dc} Mean	218.8 V	184.0 V	224.1 V

In the above-mentioned Table 6.1, three different PWM techniques have been compared based on different parameters. A particular gain of $G = 1.7$ has been chosen for the comparison purpose. For a particular gain, different modulation indexes (M) can be observed for different PWM techniques. And that can be found by equations (6.46), (6.59), and (6.75) respectively. It is observed that the modulation index in the case of MBC is higher enough compare to SBC

and MCBC at a fixed gain. Next is peak to the peak inductor current (ΔI_L), SBC and MCBC are almost the same but in the case of MBC, it is the maximum as the current is not smooth over there, which can be observed in Figure 7.6 with the 6th frequency harmonics. In the case of the boost factor (B), we are getting a high boost factor in SBC mode followed by MCBC and MBC. It can be said that although getting the highest boost factor in the case of SBC, this method is not in use significantly, because of severe voltage stress. It is seen that voltage stress (V_s) across the switches is very close to one another for MBC and MCBC but large in the case of SBC. Inductor voltage is very much important as, at NST mode in doctor voltage (V_L) adds up with the source voltage and a voltage greater than the source voltage can be observed. And here MBC is having a high voltage across the inductor among all. V_{dc} or the DC link voltage the other hand is the voltage that we get after the Z-Source network and before the switches. And at the last column, it can be observed that DC link voltage in the case of MBC is more compared to others. And this voltage is going to reflect the output side of the inverter. That means using the MBC at the same gain a more output voltage can be achievable.

CHAPTER 7
SLIDING MODE CONTROL

7.1 SUPER TWISTING CONTROLLER FOR Z-SOURCE INVERTER

The plant and the mathematical model do not agree in most of the cases. This could be caused by external disturbances, changes in plant parameters, etc. And due to these kinds of problems control law design is a difficult task. There are many other types of control methods, but PI control method is one of the oldest. And it is very much simple to understand and apply. However, because this is a linear control mechanism, it does not give an adequate performance in all operating modes. On the other hand, a non-linear controller reduces order compensated dynamics, resilience, and finite-time convergence. In control system SMC is a non-linear control strategy is very effective in the creation of reliable controller for complicated setup. It forces the system to slide along a cross-section of the system's normal behaviour.

Figure 7.1, represents the Block diagram of the sliding mode control system for the DC side of ZSI i.e., DC link voltage (Vdc). In this case, SBC has been used as a modulation method. Here in Figure 5.1, it can be seen that there are two envelopes V+ and V-. Talking about V+ it is equal to modulation index M. Now as $M = 1 - Dst$ so, $V+= 1 - Dst$ and $V-= Dst - 1$ respectively. Fig 7.1 represents the inverter switching controller block diagram. Where it can be seen that using a sliding surface and control only D_{st} has been found out and modulation index M, can find out by D_{st} itself.

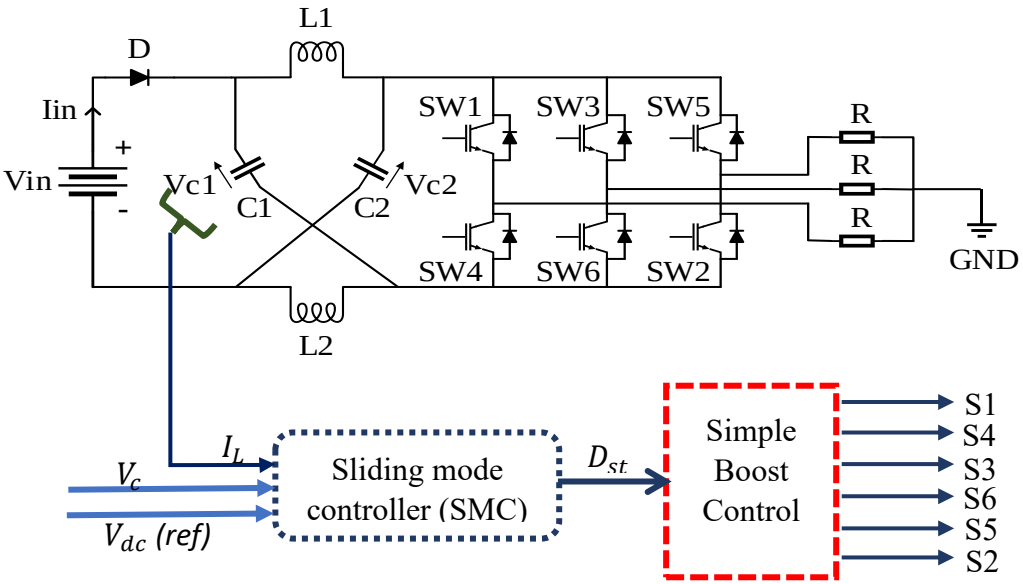

Figure 7. 1 Block diagram of second-order sliding mode control (SOSM) with ZSI circuit

7.2 SLIDING SURFACE DESIGN

After applying the average model of the ZSI and Kirchhoff's law in both NST and ST states in Figure 6.5 and Figure 6.6 we get,

$$C\frac{dV_{c1}}{dt} = I_L - 2 \cdot D_{st} \cdot I_L - M \cdot Iload \tag{7.1}$$

Here,

$$Iload = \frac{V_{dc}^* \cdot V_{c1}}{R_L \cdot V_{c1}^*} \tag{7.2}$$

From equation (6.1) and (6.2) it can be concluded that,

$$C\frac{dV_c}{dt} = I_L - 2 \cdot D_{st} \cdot I_L - M \cdot \frac{V_{dc}^* \cdot V_c}{R_L \cdot V_c^*} \tag{7.3}$$

Putting equation $M = (1 - D_{st})$ in (7.3) one has,

$$C\frac{dV_c}{dt} = I_L - 2 \cdot D_{st} \cdot I_L - (1 - D_{st}) \cdot \frac{V_{dc}^* \cdot V_c}{R_L \cdot V_c^*} \tag{7.4}$$

$$L\frac{dI_L}{dt} = D_{st}(2 \cdot V_c - V_{in}) + (V_{in} - V_c) \tag{7.5}$$

From the above equation, it can be said that the Dst and M are actually the control input. But here we are only taking the Dst as the control input. Modulation index (M) will automatically be controlled as Dst is controlled as, $M = 1 - D_{st}$

The control objective is to regulate the capacitor voltage to the desired value, we consider the following variables:

$$e_1(t) = I_L\ ,\ e_2(t) = V_c^* - V_c \tag{7.6}$$

$$\text{And } e_3(t) = \int (V_c^* - V_c)dt \tag{7.7}$$

Where $Vc^*$is the reference voltage of $V_{c_1}$and from equation (6.1) $V_{c_1} = V_c$

So, as the matrix from it can be written as,

$$\begin{bmatrix} \frac{de_1}{dt} \\ \frac{de_2}{dt} \\ \frac{de_3}{dx} \end{bmatrix} = \begin{bmatrix} \frac{(2 \cdot V_c - V_{in})}{L} \\ \frac{2 \cdot I_L}{C} - \frac{V_{dc}^* \cdot V_c}{R_L \cdot V_c^* \cdot C} \\ 0 \end{bmatrix} \cdot D_{st} + \begin{bmatrix} \frac{V_{in} - V_c}{L} \\ \frac{V_{dc}^* \cdot V_c}{R_L \cdot V_c^* \cdot C} - \frac{I_L}{C} \\ V_c^* - V_c \end{bmatrix} \tag{7.8}$$

From equations (7.6) and (7.4) it can be written as,

$$\frac{de_2}{dt} = 0 - \frac{dV_c}{dt} \tag{7.9}$$

$$\frac{de_2}{dt} = -\frac{1}{C}\left\{I_L - 2 \cdot D_{st} \cdot I_L - (1 - D_{st}) \cdot \frac{V_{dc}^* \cdot V_c}{R_L \cdot V_c^*}\right\} \tag{7.10}$$

Now sliding surface can be obtained as:

$$S(t) = a_1 \times e_1(t) + a_2 \times e_2(t) + a_3 \times e_3(t) \tag{7.11}$$

where a1, a2 and a3 are the design parameters to maintain the sliding motion. Now the design objective is to formulate an equivalent control law ($D_{st_{(eq)}}$), that can be obtained by making $\frac{ds}{dt} = 0$

$$\frac{dS}{dt} = a_1 \times \frac{de_1}{dt} + a_2 \times \frac{de_2}{dt} + a_3 \times \frac{de_3}{dt} \tag{7.12}$$

Now substituting the values of $\frac{de_1}{dt}, \frac{de_2}{dt}, \frac{de_3}{dt}$ and $D_{st_{(eq)}}$ can be obtained as:

$$D_{st_{(eq)}} = \frac{a_1 C R_L V_c^* (V_{in} - V_c) + a_2 L (V_{dc}^* V_c - R_L V_c^* I_L)}{a_2 L (V_{dc}^* V_c - 2 R_L V_c^* I_L + a_1 C R_L V_c^* (V_{in} - 2V_c)}$$

$$+ \frac{C L R_L V_c^* (a_3 V_c^* - a_3 V_c)}{a_2 L (V_{dc}^* V_c - 2 R_L V_c^* I_L) + a_1 C R_L V_c^* (V_{in} - 2V_c)} \tag{7.13}$$

Practically the value of $D_{st_{(eq)}}$ must lie in between 0 to 0.4. To enhance the robustness of the system we used the reaching law based on the super twisting algorithm. Hence,

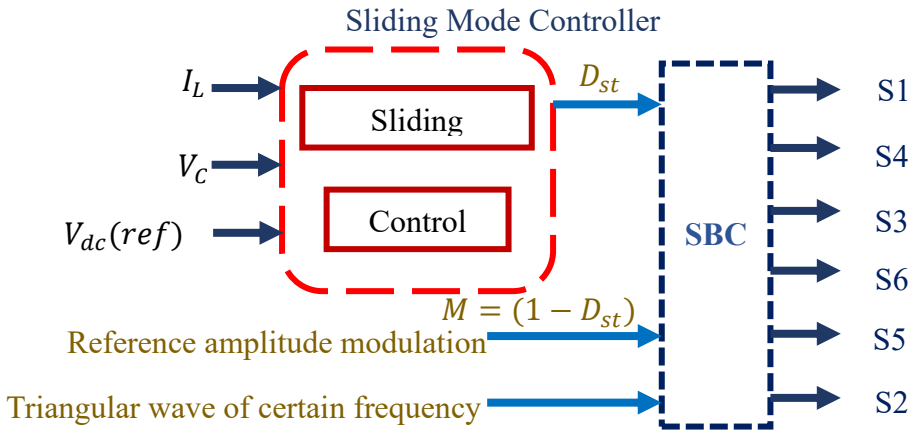

Figure 7. 2 Block diagram of the Inverter switching controller

$$\frac{dS}{dt} = -k_1|S(t)|^{0.5} sign\big(S(t)\big) - k_2 \int sign\big(S(t)\big)dt \tag{7.14}$$

Thus, the overall control law (D_{st}) can be obtained as:

$$D_{st_{eq}} = \frac{a_1 C R_L V_c^* (V_{in} - V_c) + a_2 L \left(V_{dc}^* V_c - R_L V_c^* I_L\right)}{a_2 L \left(V_{dc}^* V_c - 2R_L V_c^* I_L\right) + a_1 C R_L V_c^* (V_{in} - 2V_c)}$$

$$+ \frac{C L R_L V_c^* (a_3 V_c^* - a_3 V_c)}{a_2 L \left(V_{dc}^* V_c - 2R_L V_c^* I_L\right) + a_1 C R_L V_c^* (V_{in} - 2V_c)}$$

$$+ \frac{-k_1 |S(t)|^{0.5} sign\big(S(t)\big) - k_2 \int sign\big(S(t)\big)dt}{a_2 L \left(V_{dc}^* V_c - 2R_L V_c^* I_L\right) + a_1 C R_L V_c^* (V_{in} - 2V_c)} \tag{7.15}$$

For simulation, we consider $a_1 = 500, a_2 = 30$ and $a_3 = -10$ and $K_1 = 1$, $K_2 = 3$ respectively.

7.3 RESULTS

Certain parameters have been taken for verifying the results that have been shown in Table 7.1.

TABLE 7. 1 MATLAB Simulink Parameters

Parameters Taken	Value
DC input Voltage (Vin)	300V
Inductors (L1=L2)	8mH
Capacitor (C1=C2)	400uF
Three-phase loads	50 Ω
Fundamental frequency (f)	50Hz
Carrier Frequency (fs)	2.1kHz

The design objective is to change the output voltage from a reference value of 350 volts to 500 volts. With the specified design parameters from Figure 7.4, it can be easily verified that the proposed SOSM control achieves the desired performance. Figure 7.3 depicts the inductor current, whereas Figure 7.5 and Figure 7.6 represent the duty ratio and modulation index respectively.

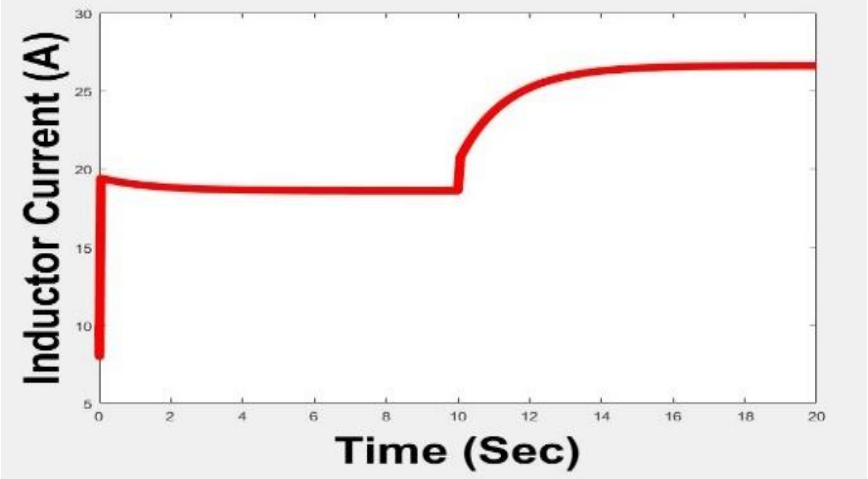

Figure 7. 3 Inductor current under SOSM

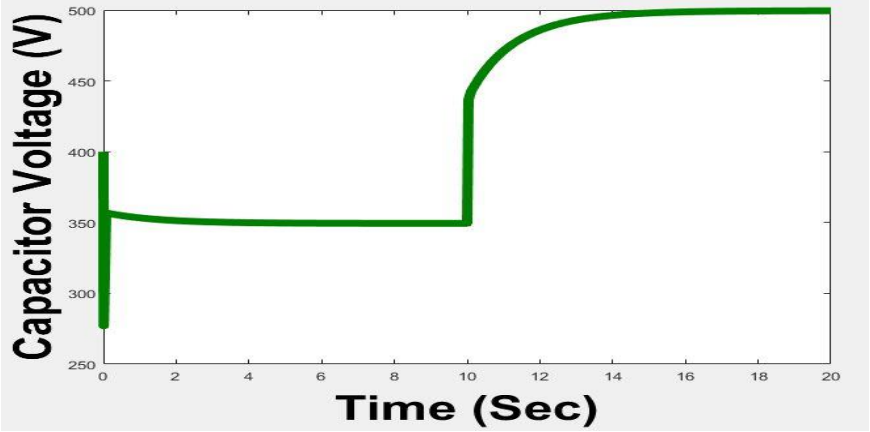

Figure 7. 4 Reference Capacitor Voltage achieved under SOSM

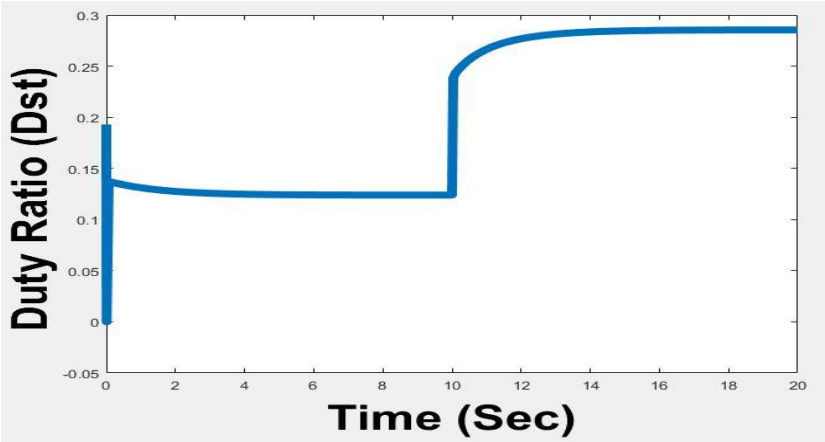

Figure 7. 5 Duty ratio D_{st} under SOSM

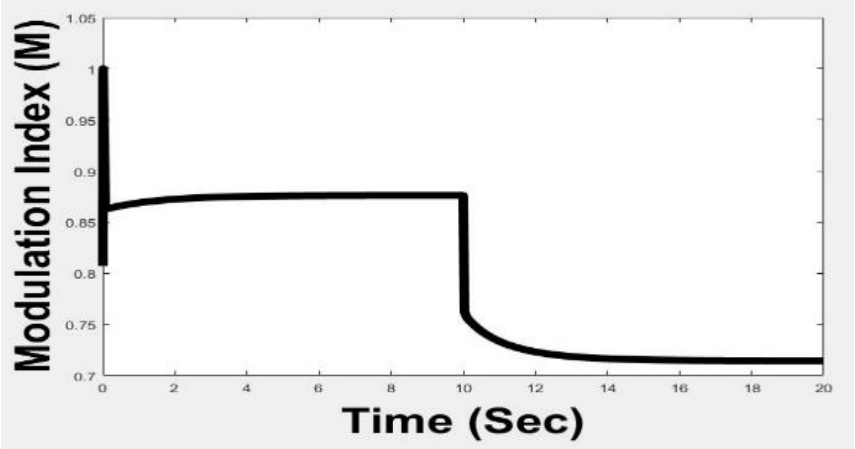

Figure 7. 6 Modulation index

Figure 7.4 represents the capacitor voltage reaching strategy. Here our first reference is 350V and the second is 500V we can see from Figure 7.4 that at approximately 2.5 sec it achieves a 350V reference state and thereafter it becomes constant for some time(sec). After approximately 10 sec it again achieves its second reference i.e., 500V. Fig 8 shows that the way inductor current is changing with respect to $D_{st}$and V_c.

As here we are controlling V_c so, the duty ratio (D_{st}) will change according. Figure 7.5 represent the way D_{st} changing to achieve the reference voltage. When the reference voltage of the capacitor reaches 350V, the time can be seen in Figure 7.5 at approximately 2.5 sec, D_{st} becomes 0.13 approximately and it becomes constant up to 10 sec after that it increases and reaches 0.28 as the capacitor voltage achieves 500V. Figure 7.6 represents the modulation index (M) which comes directly from D_{st}.

CHAPTER 8
SIMULATION AND EXPERIMENTAL RESULTS

8.1 SIMPLE BOOST CONTROL METHOD SIMULINK RESULTS

To verify the validity of the above-proposed method, MATLAB Simulink has been used. The system has been simulated at a 0.09-sec time frame.

Certain parameters have been taken for verifying the results that have been shown in TABLE 8.1.

TABLE 8. 2 MATLAB Simulink Parameters For all techniques

Parameters Taken	Value
DC input Voltage (V_{in})	130V
Inductors (L_1, L_2)	1mH
Capacitor (C_1, C_2)	330uF
Three-phase balanced loads	25 Ω
Fundamental frequency (f)	50Hz
Carrier Frequency (f_s)	2.1kHz
Modulation index (M)	0.95

Here, the simulation of SBC has been with a modulation index of 0.95 and with a relation between $M$and the D_{st}, D_{st} becomes 0.05 which is quite small. As a result, a small gain has been observed.

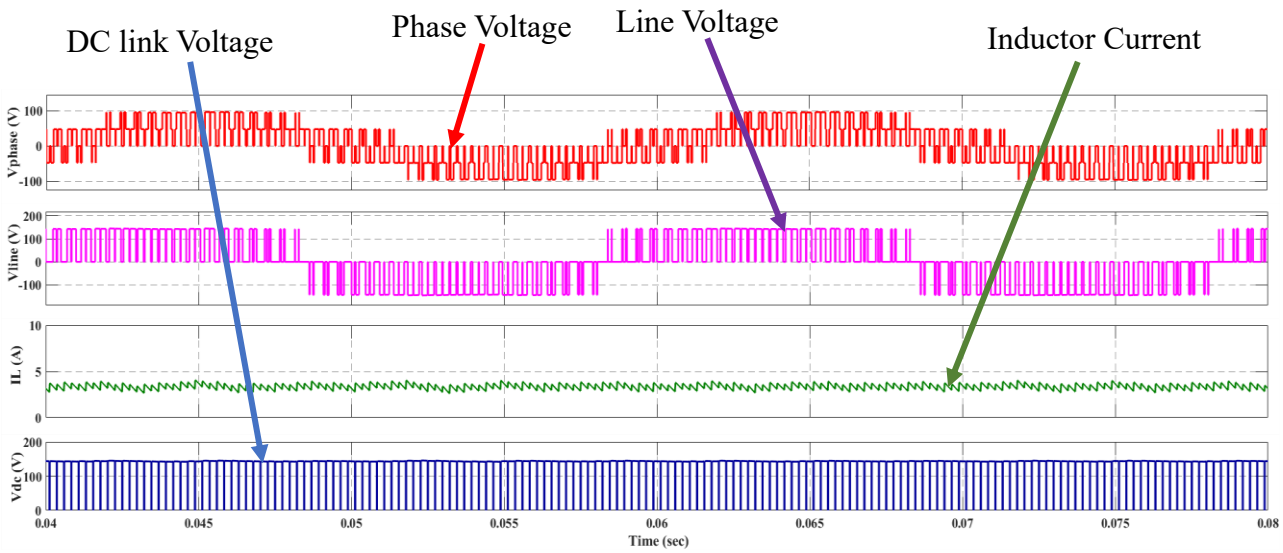

Figure 8. 7 Simulation waveforms V_{phase}, V_{line}, I_L *and* V_{dc} with SBC

In Figure 8.1 for SBC different waveforms have been analysed in Simulink i.e., DC link voltage, current across inductor current L_1, and also the phase and line voltage across the load. Here the DC link voltage is nothing but the voltage stress across the switch i.e., when the switch is in OFF condition the reverse voltage is applied across the switch. It can also be observed that a smooth inductor current waveform is achieved. Also, the charging and discharging of the inductor can be seen through the inductor current waveform, i.e., at shoot-through, the inductor charges, and at non-shoot through the inductor discharges. From Figure 8.2. both the capacitor voltage is the same and that is true according to equation (6.1).

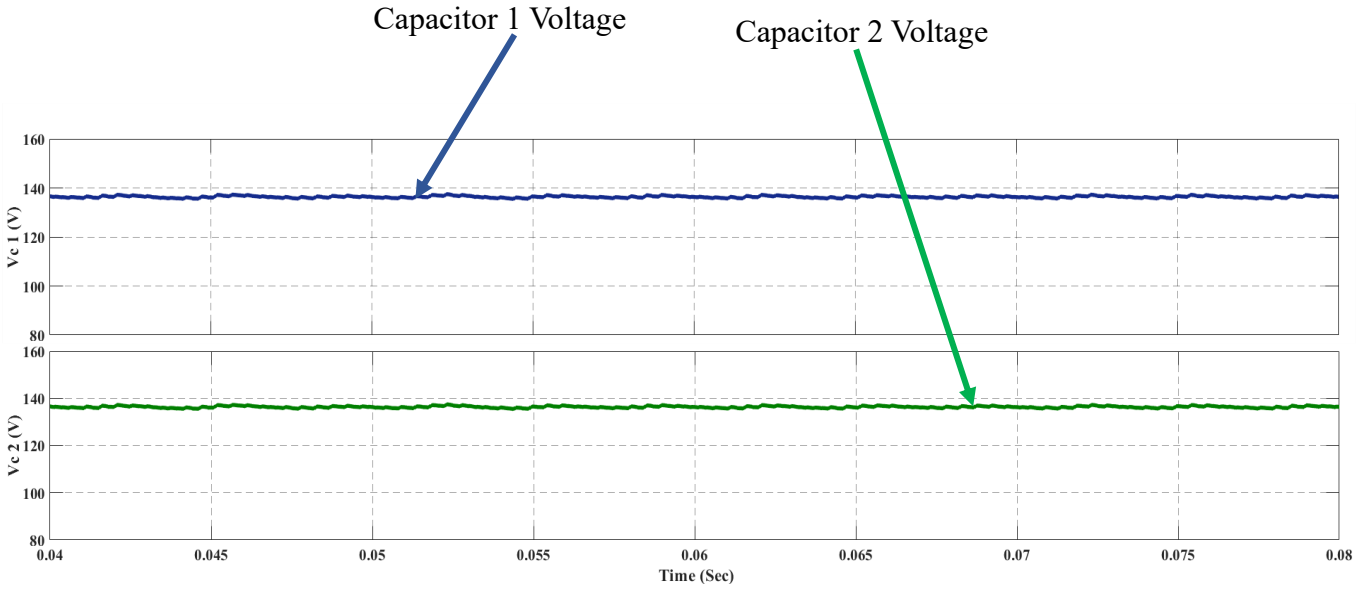

Figure 8. 8 Simulation waveform of V_{c_1} *and* V_{c_2} respectively

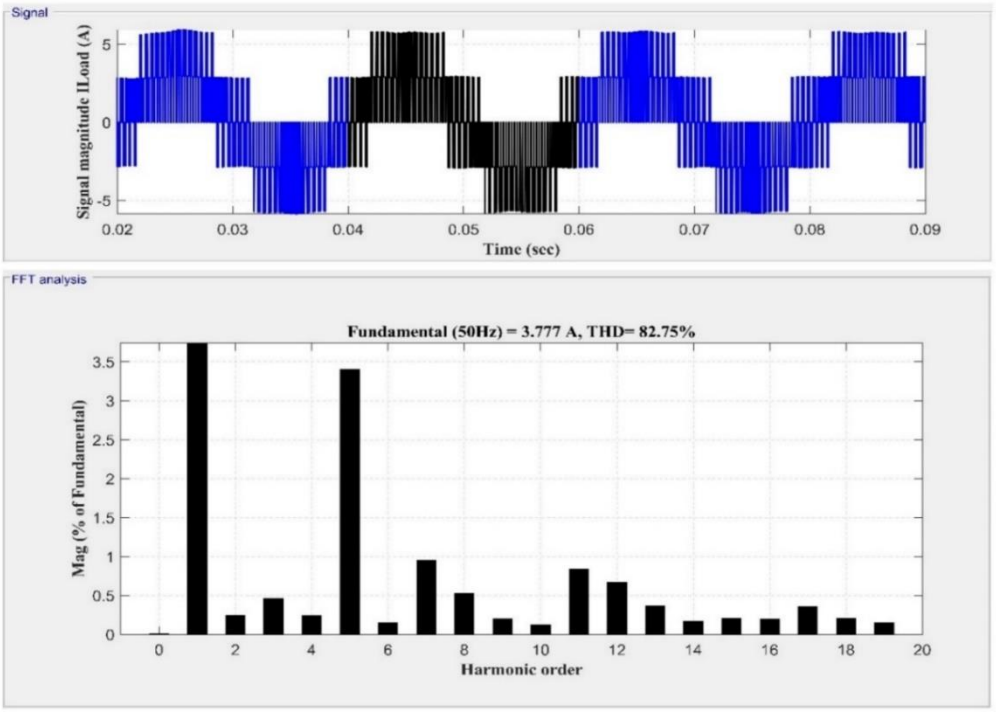

Figure 8. 9 FFT analysis of Load current I_{Load} using SBC

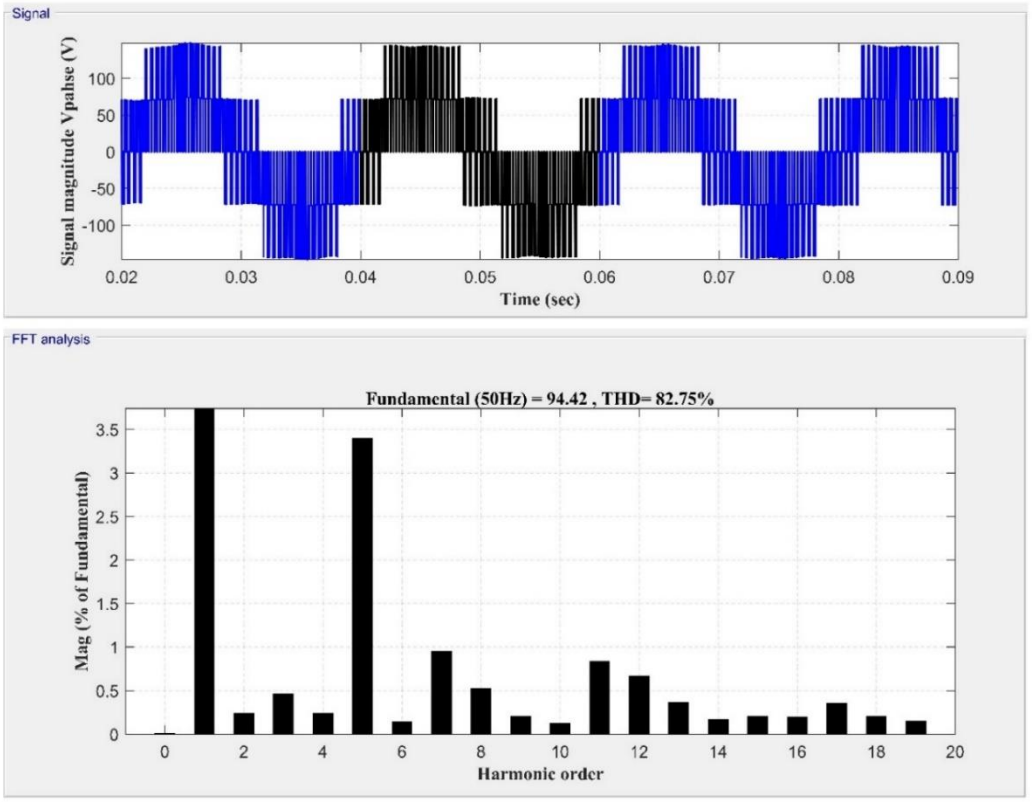

Figure 8. 10 FFT analysis of phase voltage V_{Phase} using SBC

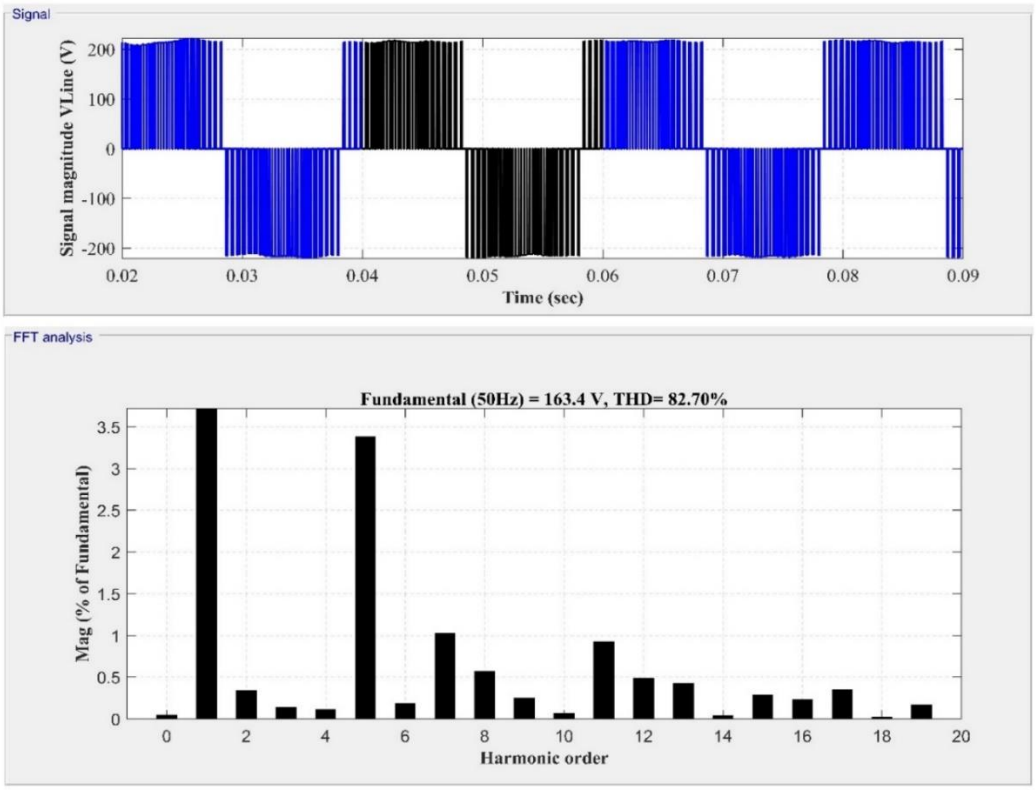

Figure 8. 11 FFT analysis of line voltage V_{Line} using SBC

The experimental result that has been simulated in MATLAB Simulink has been represented in Figures 8.1, 8.2, 8.3, 8.4, and 8.5 respectively. And the validity of the control method has been verified. From Figure 8.3 to Figure 8.5 total harmonic distortion of load current, phase voltage, and line current. Here can be observed that the fundamental harmonic is high and after that, the 5^{th} harmonic is at the higher side and from there it is decreasing as we are going towards the higher harmonics in each of the analyses.

8.2 MAXIMUM BOOST CONTROL METHOD SIMULINK RESULTS

To verify the validity of the above-proposed method, MATLAB Simulink has been used. The system has been simulated at a 0.09-sec time frame.

Here, the simulation of MBC has been with a modulation index of 0.95 and with a relation between M and the D_{st}, D_{st} becomes 0.2139 from equation (6.35) which is quite high. As a result, a high gain has been observed.

In Figure 8.6 for MBC different wave has been analysed in Simulink i.e., Vdc, current across inductor current, and also the phase and line voltage across the load. Here the DC link voltage is nothing but the voltage stress across the switch i.e., when the switch is in OFF condition the reverse voltage is applied across the IGBT. Here smooth current can't be

observed. In Figure 8.6 it can be observed that the current here is moreover with the 6^{th} frequency harmonics.

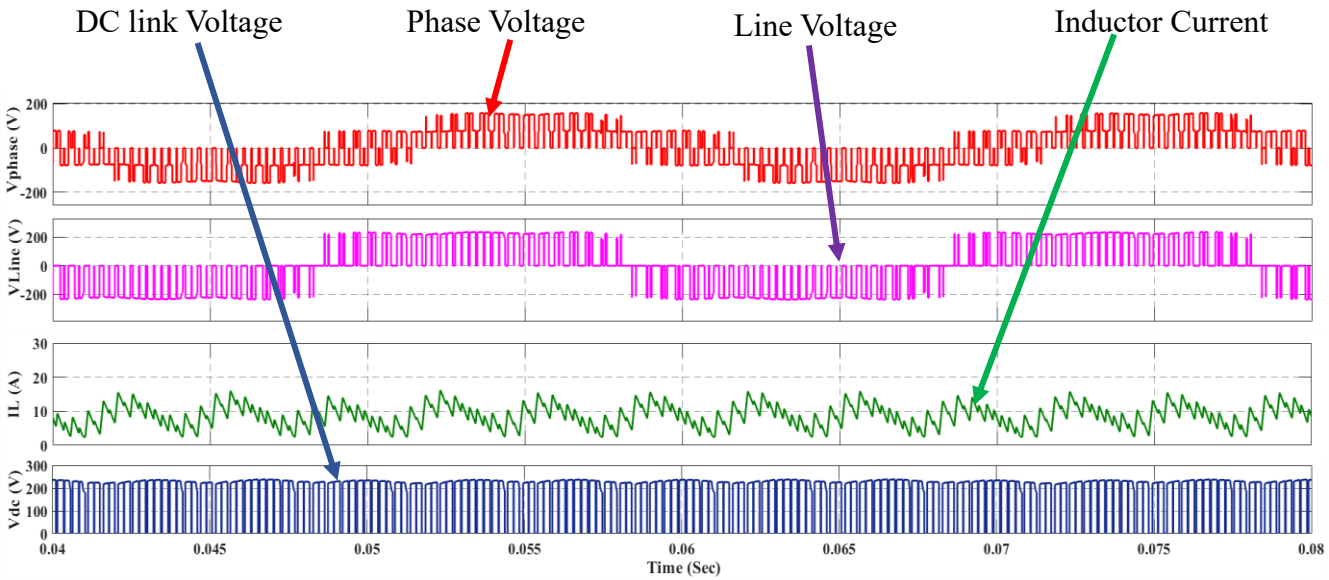

Figure 8. 12 Simulation waveforms V_{phase}, V_{line}, I_L *and* V_{dc} with MBC

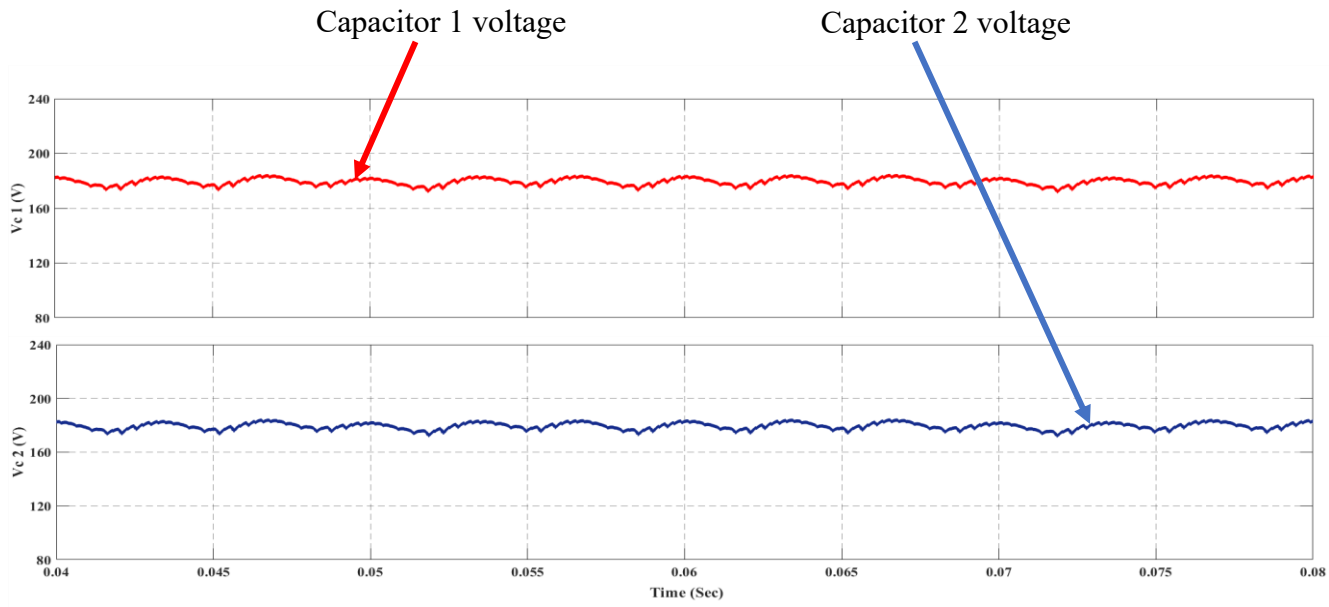

Figure 8. 13 Simulation waveforms of V_{c_1} *and* V_{c_2} respectively

From Figure 8.7. both the capacitor voltage is the same. That is true according to the main equation (6.1).

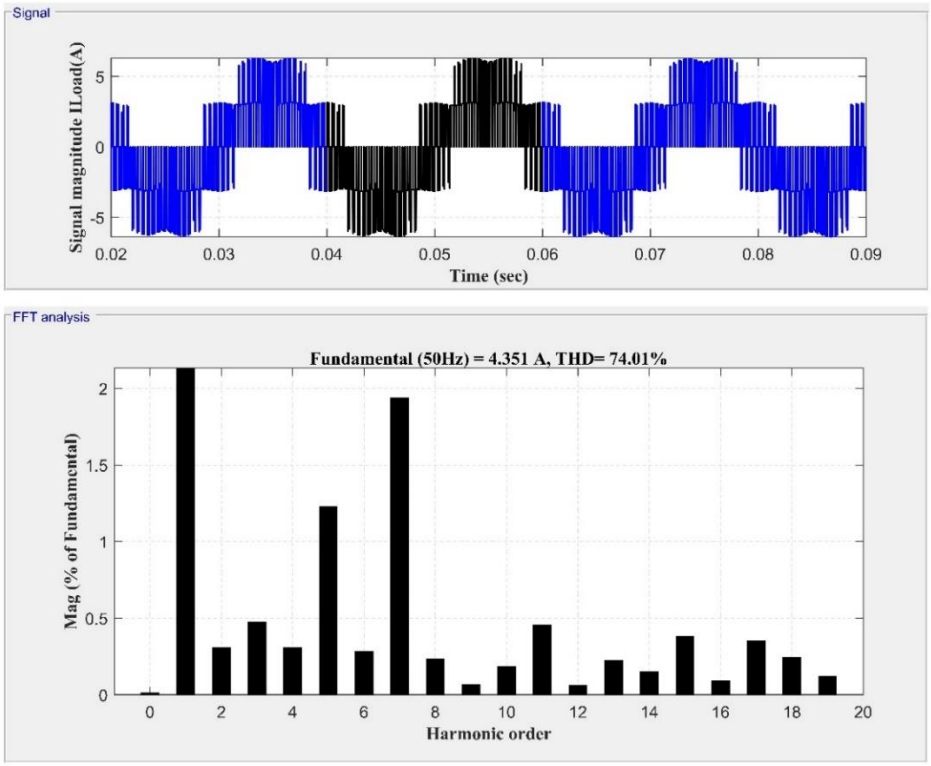

Figure 8. 14 FFT analysis of load current I_{Load} using MBC

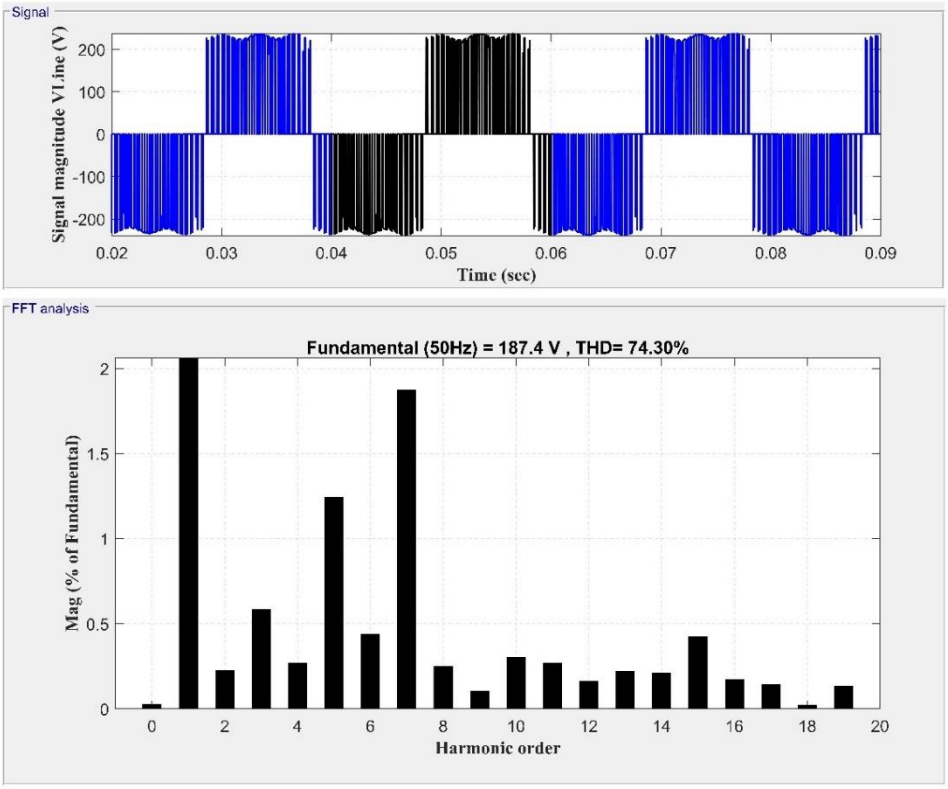

Figure 8. 15 FFT analysis of line voltage V_{Line} using MBC

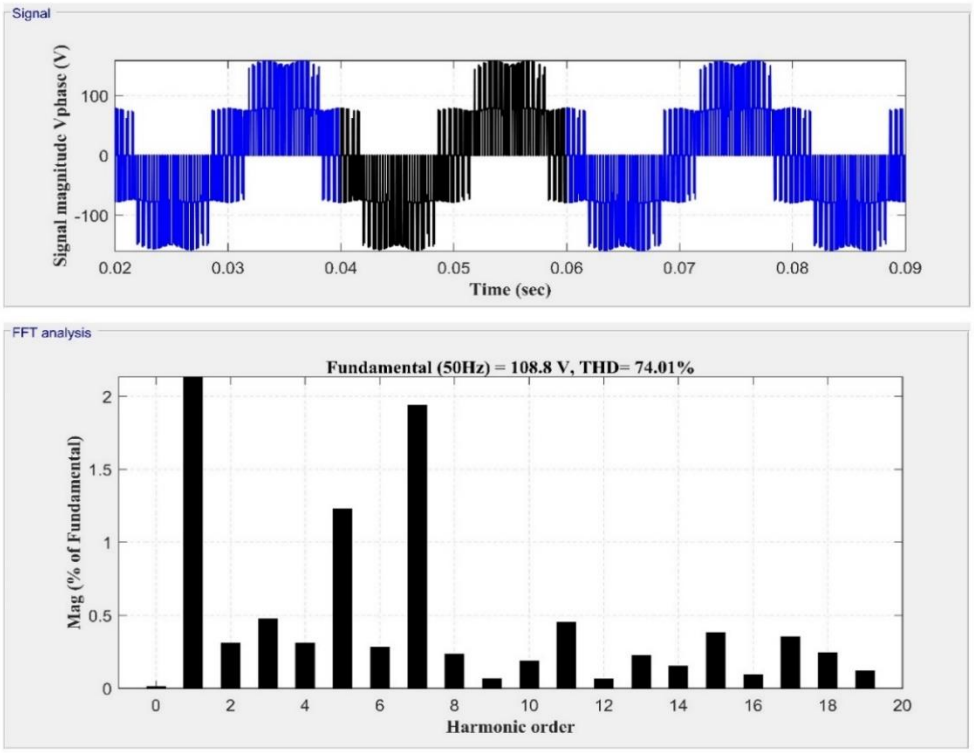

Figure 8. 16 FFT analysis of phase voltage V_{phase} using MBC

The experimental result that has been simulated in MATLAB Simulink has been represented in Figures 8.6, 8.7, 8.8, 8.9, and 8.10 respectively. And the validity of the control method has been verified. Figures 8.8, 8.9, and 8.10 THD analyses have been shown. Here we are using the unique modulation techniques so it can be observed that we getting a 7^{th} harmonic that is higher than the 5^{th} harmonic. And that is not there when talking about the traditional modulation technique.

8.3 MAXIMUM CONSTANT BOOST CONTROL METHOD SIMULINK RESULTS

To verify the validity of the above-proposed method, MATLAB Simulink has been used. The system has been simulated at a 0.09-sec time frame.

Here, the simulation of MCBC has been with M of 0.95 and with the relation between modulation index and the D_{st}, D_{st} becomes 0.1772 which is slightly small. As a result, a medium gain has been observed at the output.

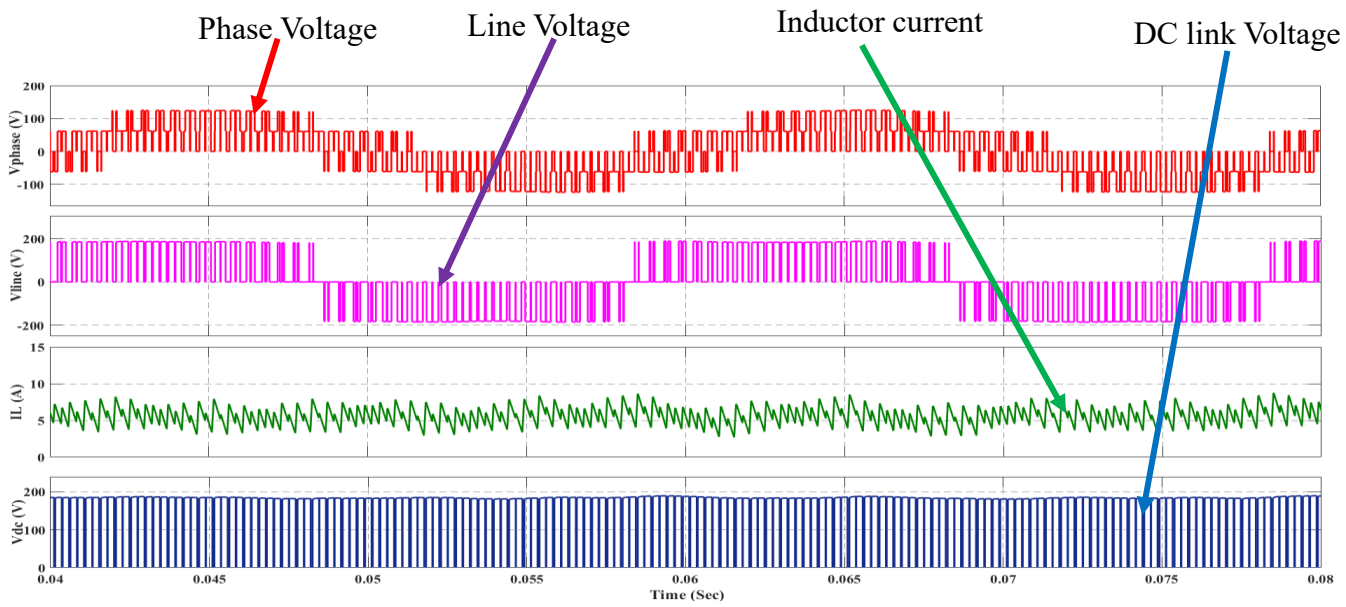

Figure 8. 17 Simulation waveforms of V_{Phase}, V_{Line}, I_L *and* V_{dc} using MCBC

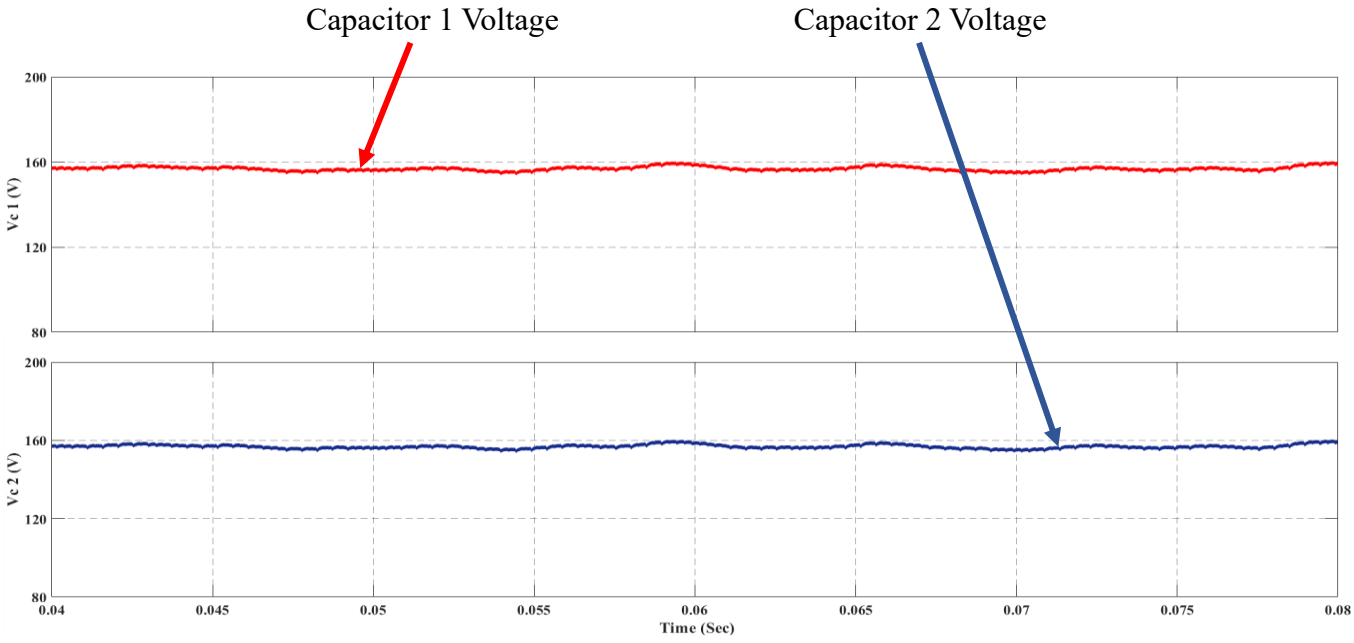

Figure 8. 18 Simulation waveforms of V_{C_1} *and* V_{C_2} using MCBC

In Figure 8.11 for MCBC different wave has been analysed in Simulink i.e., DC link voltage, current across inductor current, and also the phase and line voltage across the load. The inductor current is smooth over here but not smoother than in the case of SBC, but smoother than the MCBC. The charging and discharging of the inductor can be observed from the waveform. From Figure 8.12 it is clear that both the capacitor voltage is the same. Again, validating the equation (6.1).

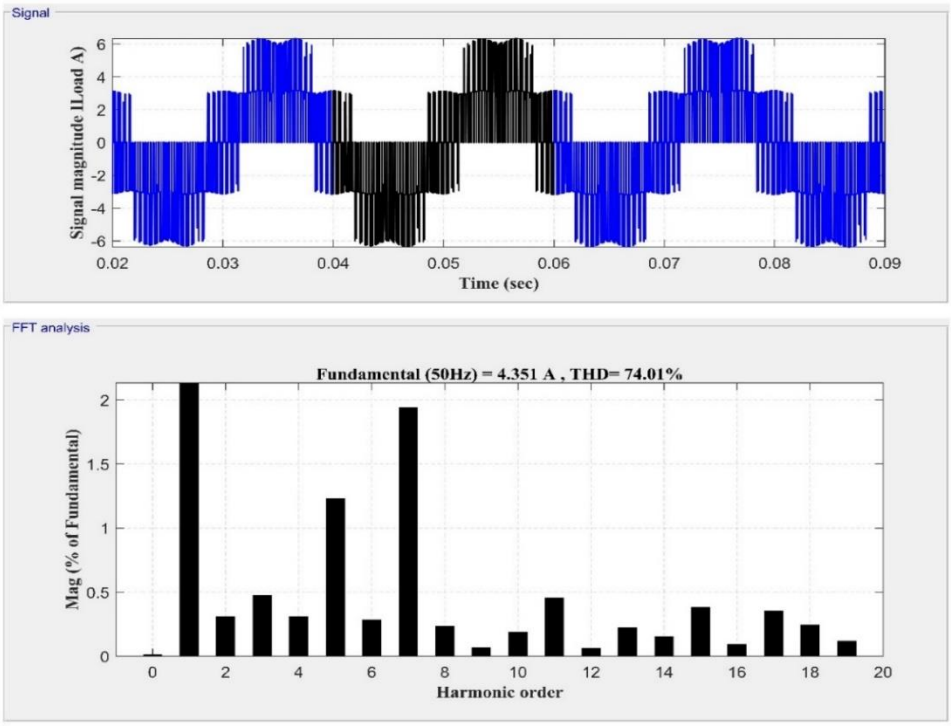

Figure 8. 19 FFT analysis of load current I_{Load} using MCBC

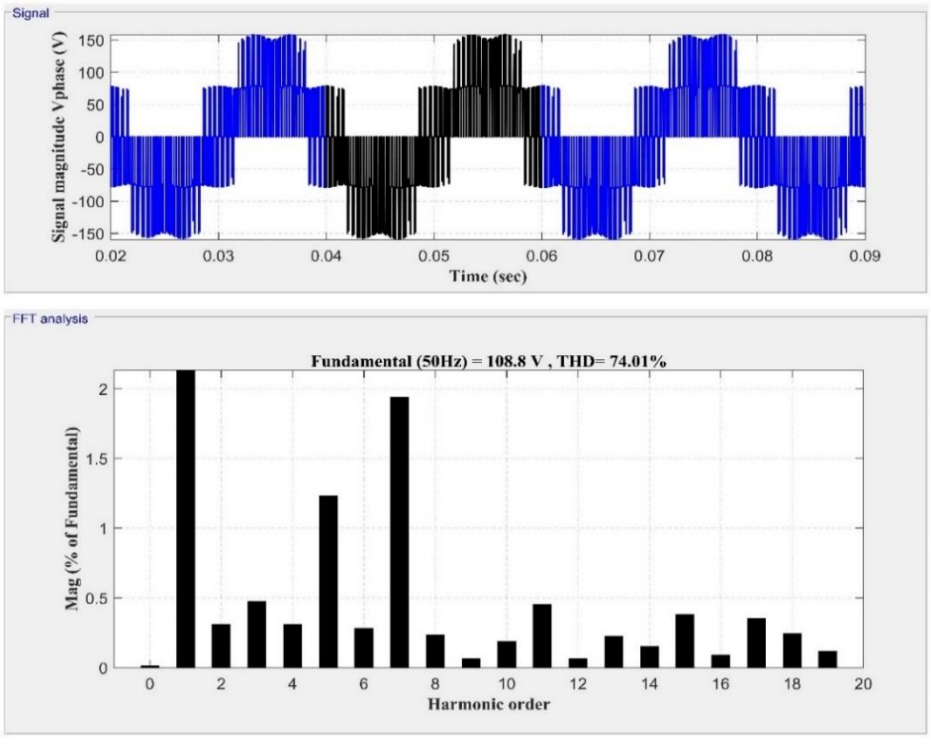

Figure 8. 20 FFT analysis of phase voltage V_{Phase} using MCBC

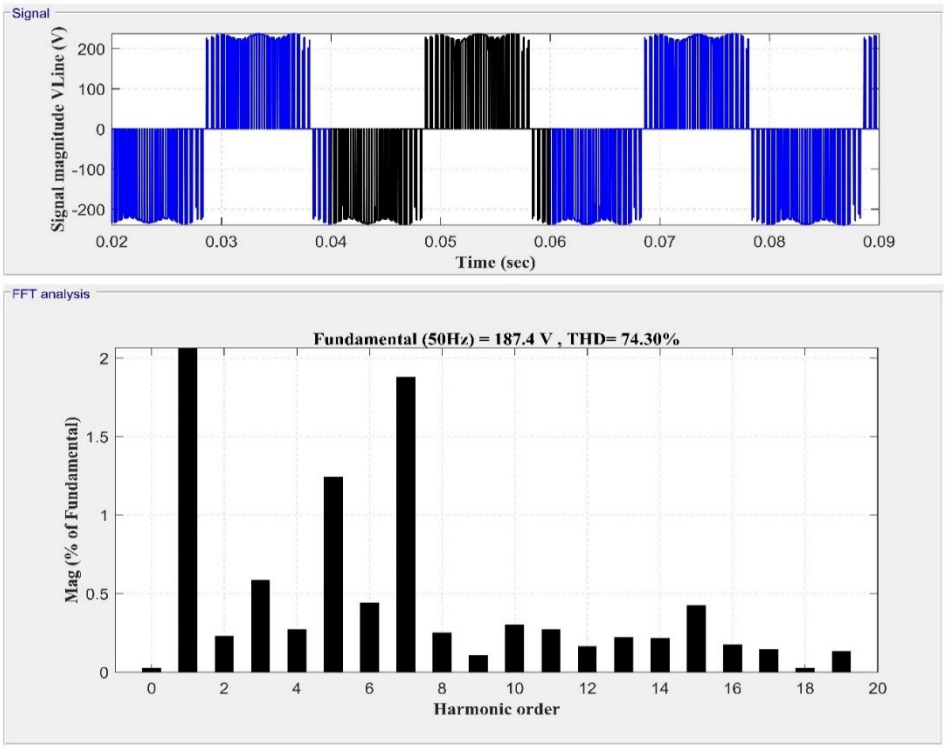

Figure 8. 21 FFT analysis of line voltage V_{Line} using MCBC

Figures 8.13, 8.14, and 8.15 show the total harmonic distortion of load current, phase voltage, and line voltage respectively. Like in the case of MBC here also the 7th harmonic is a bit more than the 5th harmonic, which can't be observed in the traditional PWM technique.

8.4 EXPERIMENTAL RESULTS AND DISCUSSION

The MATLAB Simulink was replaced by the hardware, where Figure 7.16 shows the driver circuit (DVC) with a microcontroller and six IGBTs. Here the microcontroller is the Texas instrument's microcontroller with C2000 series with serial no. TMS320F28335. DVCs are connected to a transformer, which gives a 12V of output voltage. The pulse that has been generated by using the microcontroller has been directly given to all six DVCs. At the input of the DVC, the pulse voltage is only 3V i.e., generated by the microcontroller. But at the output side of the DVC, the voltage we are getting is 12V, and that is absolutely fine to make ON the IGBTs. There is a rectifier circuit built with each of the DVCs that is converting the 12V AC to 12V DC and we are getting that voltage at the output side of the DVCs where we are getting the pulses and that is sufficient to ON the IGBTs.

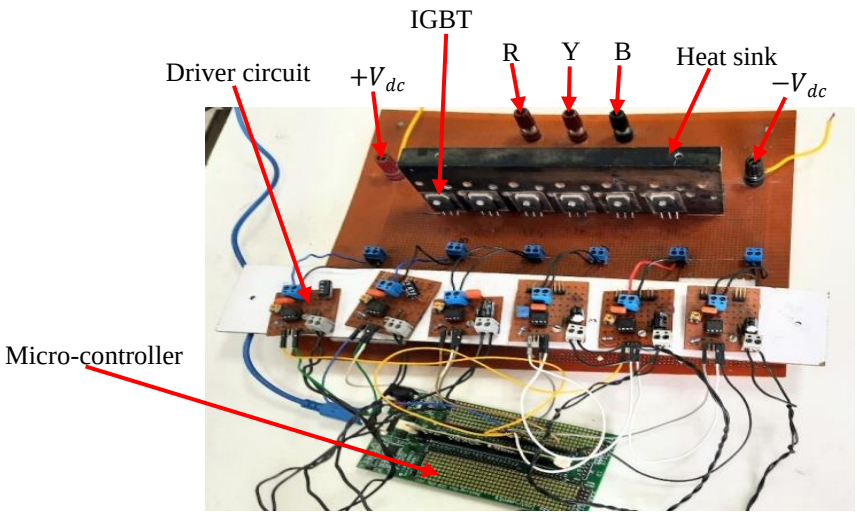

Figure 8. 22 Driver circuits

Talking a bit about the microcontroller TMS320F28335 with the series C2000, it contains up to 18 PWM outputs, and that is enough to control the power converters. According to our microcontroller among the 18 PWM output, only 12 are ePWM modules that can be used in Simulink to program the microcontroller to generate pulses at the output. The 12 ePWM modules have been shown in TABLE 8.2**.**

TABLE 8. 3 ePWM pins and GPIO pins of micro-controller

ePWM Modules	**Module Outputs(SIMULINK)**	**GPIO Pins**
ePWM1	ePWM1A	GPIO00
	ePWM1B	GPIO01
ePWM2	ePWM2A	GPIO02
	ePWM2B	GPIO03
ePWM3	ePWM3A	GPIO04
	ePWM3B	GPIO05
ePWM4	ePWM4A	GPIO06
	ePWM4B	GPIO07
ePWM5	ePWM5A	GPIO08
	ePWM5B	GPIO09
ePWM6	ePWM6A	GPIO10
	ePWM6B	GPIO11

Here in Simulink, we have used ePWMA as well as ePWMB series. ePWMA has been used for PWM techniques where we are comparing the sine wave with the triangular wave and

ePWMB has been used for comparing the DC i.e., constant with the triangular wave to generate shoot-through. Here the uniqueness of the ePWM module is that it will generate the triangular wave itself. We just have to give the sinusoidal wave and need to change some of the settings to generate perfect SPWM and similarly with the DC constant. So, as we are having six IGBTs & we took the general-purpose input-output (GPIO) port as, GPIO00, GPIO02, GPIO04, GPIO06, GPIO08, and GPIO10. Where GPIO00 is used for switch 1, GPIO02 is used for switch 4, GPIO04 is used for 3, GPIO06 is used for switch 6, GPIO08 is used for switch 5 and GPIO10 has been used for switch 2.

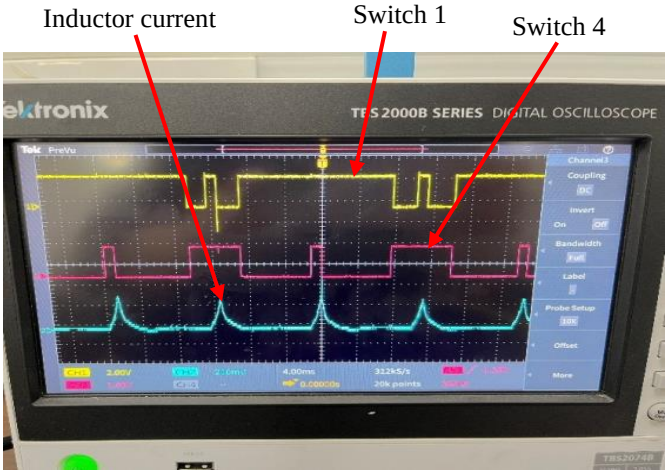

Figure 8. 23 1,4 and Inductor current

Figure 8.17 shows, how the ST is happening in the case of Switch 1 and 4 for example. The yellow colour pulse is for switch 1 and the pink colour pulse represents switch 4. The blue colour waveform is for I_L i.e., inductor current. It can be observed that whenever the ST is occurring that time both the switches are ON, and the inductor is charging, and after the ST, an NST state occurs where none of the two switches are ON together and the inductor discharges.

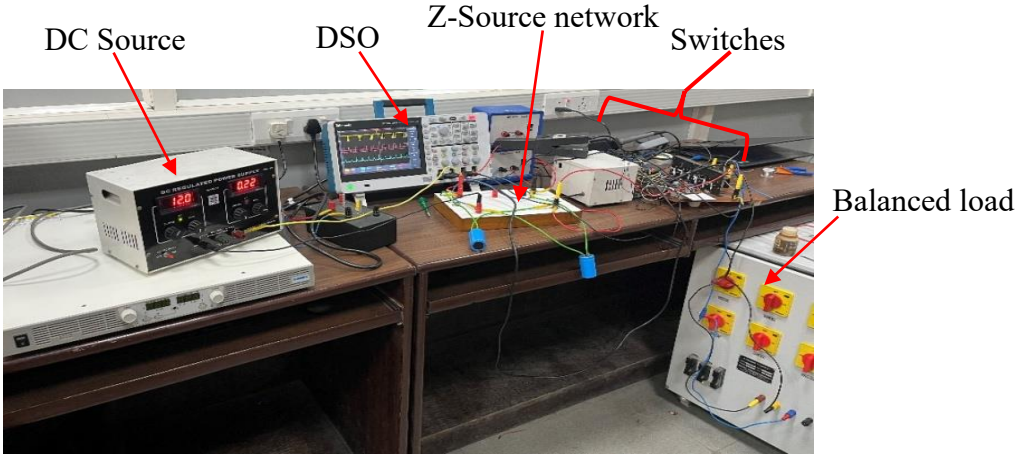

Figure 7. 24 ZSI setup

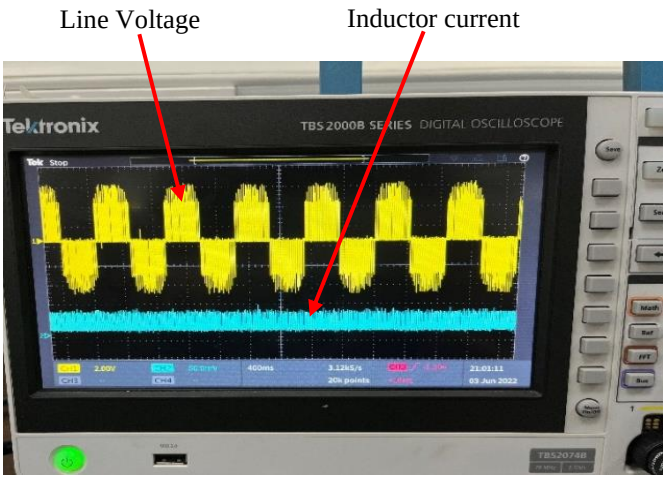

Figure 8. 25 Line voltage with inductor current

Figure 8.19 shows the line voltage (V_{line}) and inductor current (I_L) respectively. Here the yellow color waveform represents the V_{line} and the blue color waveform represents the I_L. Here it can be observed that we are getting a balanced waveform like we were getting in Simulink. The input voltage over here is 4V and the line voltage shown in this Figure 8.19 is 7-8V approximately hence it can be seen that using the Z-source network we can increase the voltage at the output.

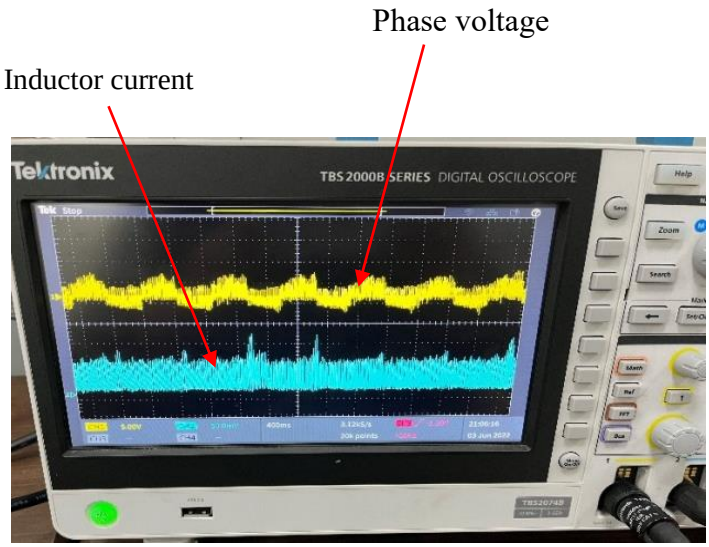

Figure 8. 26 Phase voltage with inductor current

Figure 8.20, represents the V_{phae} with the I_L. Here in every case, we have taken a load of 25 Ω. Here the yellow colour represents the phase voltage waveform and down blue colour waveform represents the I_L.

The sample time that has been taken over here is $5 \times 10^{-6}\ sec$. Sine wave block that has been used in case of Simulink there also we need to change the sample time to the above-mentioned time. We also need to change the POWERGUI block settings, i.e., we have to change the continuous-time to discrete-time with the sample time mentioned above here. This is a very much important step because the microcontroller cannot work in continuous time.

CHAPTER 9
CONCLUSION

In this report, different topologies of ZSIs and its PWM techniques are discussed in detail. A second order sliding mode control algorithm is developed for automatic tracking of modulation index and shoot through duty ratio for simple boost control technique. Constraints of conventional inverters (VSIs and CSIs) are removed by inserting an Impedance network between DC source and inverter switches. It is suitable for all power converters i.e., AC-AC, DC-DC, AC-DC, and DC-AC with suitable modifications. The key merits of ZSI are: (i)A broad range of output line voltage, conceptually $0\ to\ \infty$. (ii) lower voltage stress (iii) Higher efficiency and reliability. Single stage buck-boost capabilities of different topologies are justified through simulation and theoretical analysis. Various control methods have been compared and discussed.

The ST injection process for simple boost, maximum boost and maximum constant boost control technique is presented. To justify the merits and suitability/comparison of different ZSIs, various mathematical derivations such as boost factor, gain, voltage stress, shoot through duty ratios, etc are presented. It has been observed that voltage stress across the IGBTs in maximum boost control technique is minimum among the three selected PWM techniques, although it suffers from sixth frequency ripple component present in the inductor current and capacitor voltages. But in simple boost control and maximum constant boost control, this problem of 6^{th} frequency ripple component is absent. Moreover, these techniques develop comparatively higher voltage stress across the switches. Out of these three control techniques, gain of maximum boost control technique is highest. THD analyses for different parameters are also given. For the generation of switching pulses, Texas instruments microcontroller TMS320F28335 has been used. Complete details of ePWM pins used and corresponding generated pulses recorded on DSOs are presented. The impedance source inverter can be used in renewable energy applications, such as electrical vehicles, PV applications, Wind energy power conversion etc.

CHAPTER 10
REFERENCE

[1] Fang Zheng Peng, "Z-source inverter," in IEEE Transactions on Industry Applications, vol. 39, no. 2, pp. 504-510, March-April 2003, doi: 10.1109/TIA.2003.808920.

[2] Fang Zheng Peng, Miaosen Shen and Zhaoming Qian, "Maximum boost control of the Z-source inverter," in IEEE Transactions on Power Electronics, vol. 20, no. 4, pp. 833-838, July 2005, doi: 10.1109/TPEL.2005.850927.

[3] M. Shen, Jin Wang, A. Joseph, F. Z. Peng, L. M. Tolbert and D. J. Adams, "Maximum constant boost control of the Z-source inverter," Conference Record of the 2004 IEEE Industry Applications Conference, 2004. 39th IAS Annual Meeting., 2004, pp. 147, doi: 10.1109/IAS.2004.1348400.

[4] X. P. Fang, Ji Min Cui, Jie Liu and Mao Yong Cao, "Detail research on the traditional inverter and Z-source inverter," 2011 International Conference on Applied Superconductivity and Electromagnetic Devices, 2011, pp. 318-321, doi: 10.1109/ASEMD.2011.6145133.

[5] M. K. Islam, M. M. Zaved, A. M. Siddiky and K. A. Al Mamun, "A comparative analysis among PWM control Z-Source Inverter with conventional PWM Inverter for induction motor drive," 2016 International Conference on Innovations in Science, Engineering and Technology (ICISET), 2016, pp. 1-6, doi: 10.1109/ICISET.2016.7856496.

[6] J. Li, J. Liu and Z. Liu, "Comparison of Z-source inverter and traditional two-stage boost-buck inverter in grid-tied renewable energy generation," 2009 IEEE 6th International Power Electronics and Motion Control Conference, 2009, pp. 1493-1497, doi: 10.1109/IPEMC.2009.5157623.

[7] https://nptel.ac.in/courses/108105066 , Prof. D. Prasad, Prof. N.K. De, Dr. D. Kastha, Prof. Sabyasachi Sengupta, IIT Kharagpur

[8] https://www.youtube.com/channel/UCVPhkP0ju-Y1uuq16-cCr9w/videos

[9] M. Shahparasti, A. Sadeghi Larijani, A. Fatemi, A. Yazdian Varjani and M. Mohammadian, "Quasi Z-source inverter for photovoltaic system connected to single phase AC grid," 2010 1st Power Electronic & Drive Systems & Technologies Conference (PEDSTC), 2010, pp. 456-460, doi: 10.1109/PEDSTC.2010.5471773.

[10] N. Noroozi and M. R. Zolghadri, "Three-Phase Quasi-Z-Source Inverter With Constant Common-Mode Voltage for Photovoltaic Application," in IEEE Transactions on Industrial Electronics, vol. 65, no. 6, pp. 4790-4798, June 2018, doi: 10.1109/TIE.2017.2774722.

[10] J. Liu, J. Wu, J. Qiu and J. Zeng, "Switched Z-Source/Quasi-Z-Source DC-DC Converters With Reduced Passive Components for Photovoltaic Systems," in IEEE Access, vol. 7, pp. 40893-40903, 2019, doi: 10.1109/ACCESS.2019.2907300.

[11] L. He, J. Nai and J. Zhang, "Single-Phase Safe-Commutation Trans-Z-Source AC–AC Converter With Continuous Input Current," in IEEE Transactions on Industrial Electronics, vol. 65, no. 6, pp. 5135-5145, June 2018, doi: 10.1109/TIE.2017.2764876.

[12] Y. Liu, B. Ge, H. Abu-Rub and H. Sun, "Hybrid Pulsewidth Modulated Single-Phase Quasi-Z-Source Grid-Tie Photovoltaic Power System," in IEEE Transactions on Industrial Informatics, vol. 12, no. 2, pp. 621-632, April 2016, doi: 10.1109/TII.2016.2524561.

[13] A. Battiston, E. -H. Miliani, S. Pierfederici and F. Meibody-Tabar, "A Novel Quasi-Z-Source Inverter Topology With Special Coupled Inductors for Input Current Ripples Cancellation," in IEEE Transactions on Power Electronics, vol. 31, no. 3, pp. 2409-2416, March 2016, doi: 10.1109/TPEL.2015.2429593.

[14] M. Nguyen, Y. Lim and S. Park, "Improved Trans-Z-Source Inverter With Continuous Input Current and Boost Inversion Capability," in IEEE Transactions on Power Electronics, vol. 28, no. 10, pp. 4500-4510, Oct. 2013, doi: 10.1109/TPEL.2012.2233758.

[15] Fan Zhang, Xupeng Fang, F. Z. Peng and Zhaoming Qian, "A new three-phase ac-ac Z-source converter," Twenty-First Annual IEEE Applied Power Electronics Conference and Exposition, 2006. APEC '06., 2006, pp. 4 pp.-, doi: 10.1109/APEC.2006.1620526.

[16] X. Fang, B. Ma, G. Gao and L. Gao, "Three phase trans-Quasi-Z-source inverter," in CPSS Transactions on Power Electronics and Applications, vol. 3, no. 3, pp. 223-231, Sept. 2018, doi: 10.24295/CPSSTPEA.2018.00022.

[17] T. -D. Duong, M. -K. Nguyen, Y. -C. Lim, J. -H. Choi and D. M. Vilathgamuwa, "A Comparison Between Quasi-Z-Source Inverter and Active Quasi-Z-Source Inverter," 2019 10th International Conference on Power Electronics and ECCE Asia (ICPE 2019 - ECCE Asia), 2019, pp. 3209-3214, doi: 10.23919/ICPE2019-ECCEAsia42246.2019.8797196.

[18] S. Singh and S. Sonar, "Space vector based PWM sequences for Z-source principal derived inverter topologies," 2018 IEEMA Engineer Infinite Conference (eTechNxT), 2018, pp. 1-6, doi: 10.1109/ETECHNXT.2018.8385336.

[19] Y. Liu, B. Ge, H. Abu-Rub and F. Z. Peng, "Overview of Space Vector Modulations for Three-Phase Z-Source/Quasi-Z-Source Inverters," in IEEE Transactions on Power Electronics, vol. 29, no. 4, pp. 2098-2108, April 2014, doi: 10.1109/TPEL.2013.2269539.

[20] S. Sonar and S. Singh, "Improved Space Vector PWM Techniques of the Three level ZSI," 2019 International Conference on Computing, Power and Communication Technologies (GUCON), 2019, pp. 508-513.

[21] S. Sonar, S. Mondal, J. Ghommam and S. Banerjee, "An Optimized Space Vector Based Switching Algorithm With Reduced Switching Transitions for Impedance Source Inverter," in IEEE Access, vol. 10, pp. 28965-28974, 2022, doi: 10.1109/ACCESS.2022.3153497.

[22] S. Ghosh, K. Sarkar, D. Maiti and S. K. Biswas, "A single-phase isolated Z-source inverter," 2016 2nd International Conference on Control, Instrumentation, Energy & Communication (CIEC), 2016, pp. 339-342, doi: 10.1109/CIEC.2016.7513738.

[23] S. Sonar and T. Maity, "Design and simulation of a novel single phase to three phase wind power converter," 2012 1st International Conference on Recent Advances in Information Technology (RAIT), 2012, pp. 725-730, doi: 10.1109/RAIT.2012.6194585.

[24] S. Singh and S. Sonar, "Improved Maximum Boost Control and Reduced Common-Mode Voltage Switching Patterns of Three-Level Z-Source Inverter," in IEEE Transactions on Power Electronics, vol. 36, no. 6, pp. 6557-6571, June 2021, doi: 10.1109/TPEL.2020.3040908.

[25] S. Sonar and T. Maity, "Z-source inverter based control of wind power," 2011 International Conference on Energy, Automation and Signal, 2011, pp. 1-6, doi: 10.1109/ICEAS.2011.6147087.

[26] R. R. Patil, S. P. Patil, S. D. Patil and A. M. Mulla, "Designing Of Z-source inverter for photovoltaic system using MATLAB/SIMULINK," 2017 International Conference on Circuit ,Power and Computing Technologies (ICCPCT), 2017, pp. 1-5, doi: 10.1109/ICCPCT.2017.8074331.

[27] S. Singh and S. Sonar, "A New SVPWM Technique to Reduce the Inductor Current Ripple of Three-Phase Z-Source Inverter," in IEEE Transactions on Industrial Electronics, vol. 67, no. 5, pp. 3540-3550, May 2020, doi: 10.1109/TIE.2019.2916298.

[28] M. A. Kumar and M. Barai, "Performance analysis of control and modulation methods of z-source inverter," 2015 IEEE International Conference on Signal Processing,

Informatics, Communication and Energy Systems (SPICES), 2015, pp. 1-5, doi: 10.1109/SPICES.2015.7091395.

[29] P. Kumar, S. Sonar and P. Shaw, "Comparative analysis of three phase ac-ac Z-source converter topologies," 2016 IEEE 1st International Conference on Power Electronics, Intelligent Control and Energy Systems (ICPEICES), 2016, pp. 1-6, doi: 10.1109/ICPEICES.2016.7853427.

[30] https://www.youtube.com/watch?v=Dg5AIy0bY1A

[31] https://www.youtube.com/watch?v=GSpH3s6K0Ic

[32] A. Das, D. Lahiri and A. K. Dhakar, "Residential solar power systems using Z - source inverter," TENCON 2008 - 2008 IEEE Region 10 Conference, 2008, pp. 1-6, doi: 10.1109/TENCON.2008.4766835.

[33] S. A. Singh, G. Carli, N. A. Azeez and S. S. Williamson, "Modeling, Design, Control, and Implementation of a Modified Z-Source Integrated PV/Grid/EV DC Charger/Inverter," in IEEE Transactions on Industrial Electronics, vol. 65, no. 6, pp. 5213-5220, June 2018, doi: 10.1109/TIE.2017.2784396.

[34] M. Li, R. Iijima, T. Mannen, T. Isobe and H. Tadano, "New Modulation for Z-Source Inverters With Optimized Arrangement of Shoot-Through State for Inductor Volume Reduction," in IEEE Transactions on Power Electronics, vol. 37, no. 3, pp. 2573-2582, March 2022, doi: 10.1109/TPEL.2021.3109672.

[35] S. Sajadian and R. Ahmadi, "Model Predictive Control of Dual-Mode Operations Z-Source Inverter: Islanded and Grid-Connected," in IEEE Transactions on Power Electronics, vol. 33, no. 5, pp. 4488-4497, May 2018, doi: 10.1109/TPEL.2017.2723358.

LIST OF PUBLICATIONS

[1] S. Maiti, S. Sonar and S. Ashraf, "Analysis and Comparison of Impedance Source Inverter with different suitable PWM approaches," 2022 6th International Conference on Intelligent Computing and Control Systems (ICICCS), 2022, pp. 321-326, doi: 10.1109/ICICCS53718.2022.9788211.

[2] S. Ashraf, S. Sonar and S. Maiti, "Impedance Source Inverter with Maximum Gain," 2022 6th International Conference on Intelligent Computing and Control Systems (ICICCS), 2022, pp. 315-320, doi: 10.1109/ICICCS53718.2022.9788128.

[3] Subha Maiti, Santosh Sonar and Subrata Banerjee, " Design and analysis of Z-Source Inverter using Simple Boost Control Method," (IEMRE-2022, accepted and presented).

[4] Subha Maiti, Santosh Sonar, Sanjoy Mondal and Rajib Malik, " A Second Order Sliding mode control of Z-Source Inverter using Simple Boost Control Method," (IEMRE-2022, accepted and presented).

ME Thesis _2022_Final

ORIGINALITY REPORT

13%	5%	12%	3%
SIMILARITY INDEX	INTERNET SOURCES	PUBLICATIONS	STUDENT PAPERS

PRIMARY SOURCES

1	Saima Ashraf, Santosh Sonar, Subha Maiti. "Impedance Source Inverter with Maximum Gain", 2022 6th International Conference on Intelligent Computing and Control Systems (ICICCS), 2022 Publication	3%
2	Subha Maiti, Santosh Sonar, Saima Ashraf. "Analysis and Comparison of Impedance Source Inverter with different suitable PWM approaches", 2022 6th International Conference on Intelligent Computing and Control Systems (ICICCS), 2022 Publication	2%
3	Yushan Liu, Haitham Abu - Rub, Baoming Ge, Frede Blaabjerg, Omar Ellabban, Poh Chiang Loh. "Impedance Source Power Electronic Converters", Wiley, 2016 Publication	1%
4	www.researchgate.net Internet Source	1%